catalysts

MDPI

Article

$PdPt_y/V_2O_5$-TiO_2: Highly Active Catalysts with Good Moisture- and Sulfur Dioxide-Resistant Performance in Toluene Oxidation

Jingjing Sun, Yuxi Liu, Jiguang Deng, Lin Jing, Minming Bao, Qinpei Sun, Linlin Li, Linke Wu, Xiuqing Hao and Hongxing Dai *

Beijing Key Laboratory for Green Catalysis and Separation, Key Laboratory of Beijing on Regional Air Pollution Control, Key Laboratory of Advanced Functional Materials, Education Ministry of China, Laboratory of Catalysis Chemistry and Nanoscience, Department of Chemical Engineering, Faculty of Environment and Life, Beijing University of Technology, Beijing 100124, China

* Correspondence: hxdai@bjut.edu.cn; Tel.: +8610-6739-6118; Fax: +8610-6739-1983

Abstract: Catalytic performance and moisture and sulfur dioxide resistance are important for a catalyst used for the oxidation of volatile organic compounds (VOCs). Supported noble metals are active for VOC oxidation, but they are easily deactivated by water and sulfur dioxide. Hence, it is highly desired to develop a catalyst with high performance and good moisture and sulfur dioxide resistance in the oxidation of VOCs. In this work, we first adopted the hydrothermal method to synthesize a V_2O_5-TiO_2 composite support, and then employed the polyvinyl alcohol (PVA)-protecting $NaBH_4$ reduction strategy to fabricate xPdPt$_y$/V_2O_5-TiO_2 catalysts (x and y are the PdPt$_y$ loading (0.41, 0.46, and 0.49 wt%) and Pt/Pd molar ratio (2.10, 0.85, and 0.44), respectively; the corresponding catalysts are denoted as 0.46PdPt$_{2.10}$/V_2O_5-TiO_2, 0.41PdPt$_{0.85}$/V_2O_5-TiO_2, and 0.49PdPt$_{0.44}$/V_2O_5-TiO_2). Among all the samples, 0.46PdPt$_{2.10}$/V_2O_5-TiO_2 exhibited the best catalytic activity for toluene oxidation ($T_{50\%}$ = 220 °C and $T_{90\%}$ = 245 °C at a space velocity of 40,000 mL/(g h), apparent activation energy (E_a) = 45 kJ/mol), specific reaction rate at 230 °C = 98.6 μmol/(g_{Pt} s), and turnover frequency ($TOF_{Noble\ metal}$) at 230 °C = 142.2 × 10^{-3} s^{-1}. The good catalytic performance of 0.46PdPt$_{2.10}$/V_2O_5-TiO_2 was associated with its well-dispersed PdPt$_{2.10}$ nanoparticles, high adsorbed oxygen species concentration, good redox ability, large toluene adsorption capacity, and strong interaction between PdPt$_y$ and V_2O_5-TiO_2. No significant changes in toluene conversion were detected when 5.0 vol% H_2O or 50 ppm SO_2 was introduced to the reaction system. According to the characterization results, we can realize that vanadium is the main site for SO_2 adsorption while PdO is the secondary site for SO_2 adsorption, which protects the active Pt site from being poisoned by SO_2, thus making the 0.46PdPt$_{2.10}$/$V_2O_5TiO_2$ catalyst show good sulfur dioxide resistance.

Keywords: palladium–platinum bimetallic nanoparticle; vanadia–titania composite support; supported noble metal catalyst; toluene oxidation; moisture resistance; sulfur dioxide resistance

check for updates

Citation: Sun, J.; Liu, Y.; Deng, J.; Jing, L.; Bao, M.; Sun, Q.; Li, L.; Wu, L.; Hao, X.; Dai, H. PdPt$_y$/V_2O_5-TiO_2: Highly Active Catalysts with Good Moisture- and Sulfur Dioxide-Resistant Performance in Toluene Oxidation. *Catalysts* **2022**, *12*, 1302. https://doi.org/10.3390/catal12111302

Academic Editor: Takeshi Ohkuma

Received: 10 September 2022
Accepted: 19 October 2022
Published: 24 October 2022

1. Introduction

Volatile organic compounds (VOCs) are important precursors of $PM_{2.5}$ and ozone that lead to atmospheric environmental problems, such as haze and photochemical smog. In the emitted VOCs, however, there are some toxic gases such as SO_2 [1]. Hence, many countries have enacted strict laws to control VOC emissions [2,3]. Among all of the methods to eliminate VOCs, catalytic oxidation is considered to be an effective pathway owing to its high removal efficiency, energy saving, and no secondary pollution [4,5]. The key issue of such a technology is the development of an efficient and stable catalyst.

It was reported that the supported noble metal catalysts were conducive to the adsorption and activation of VOCs and oxygen, thus exhibiting high low-temperature activities

for VOC oxidation [6]. Among the noble metal catalysts, the supported Pt nanoparticles (NPs) performed well in the oxidation of toluene [7]. For example, previous studies demonstrated that Pt/CeO_2, Pt/TiO_2, and Pd-Pt/SiO_2 showed good catalytic activities for toluene oxidation [7–9]. However, SO_2 is often adsorbed on the noble metal active site, which deactivates the catalyst. For instance, SO_2 could adsorb at the active site of PdO to form the PdO-SO_x species, hence affecting the catalytic activity [10,11]. To solve this problem, two main strategies are developed to improve the SO_2 resistance of a catalyst. One is to dope another metal to modulate the outermost electron number of the active component so that the active component becomes less susceptible to SO_2 or SO_3 adsorption; the other is to add an auxiliary agent that competes with the active component for SO_2 or SO_3 adsorption [12–16]. Due to the interaction between support and active site, sulfur resistance of a catalyst can be improved after suitable treatment of the support. It was reported that metal oxides might bind sulfur dioxide to form sulfides more easily than precious metals [17]. Hoyos et al. [18] observed that the deactivation rate of PdO loaded on Al_2O_3 was much lower than that of PdO loaded on SiO_2, since Al_2O_3 was more likely to form sulfate. In general, the commonly used acidic oxide supports include TiO_2, Al_2O_3, and V_2O_5, and etc. Over V_2O_5, sulfur dioxide can be readily oxidized into sulfur trioxide [19]. TiO_2 is widely used for photocatalytic reactions due to its weak alkalinity, non-toxicity, and suitable band-gap structure. For example, Bahnemann and coworkers [20–22] prepared Rh NPs photodeposited on TiO_2 and found that the UV-active TiO_2 was a suitable support for the visible-light-driven photocatalytic selective dehydrogenation of N-heterocyclic amines. They also used the surface-grafted and commercially available UV-100 (TiO_2) photocatalyst to photocatalyze the selective aerobic dehydrogenation of N-heterocycles under the visible-light illumination and proposed that the basic reactant was adsorbed at the Lewis acid sites on the TiO_2 surface, thus improving the selectivity and yield to over 90% [21], respectively. The same group synthesized a nanocomposite (WO_3/TiO_2) of WO_3 and TiO_2 with its surface modified by Fe(III) nanoclusters to efficiently utilize visible light for the degradation of indoor air pollutants, and they found that the Fe(III)-grafted WO_3/TiO_2 nanocomposite exhibited extremely high photocatalytic activity and stability as compared with the un-grafted WO_3/TiO_2 composite, which was due to the fact that the surface-grafted Fe(III) ions can suppress the recombination of e^-/h^+ pairs [22]. It is expected that surface area, acidity, and SO_2 resistance of a support can be modified by making it into a binary metal oxide composite. For example, the composite oxides (e.g., TiO_2-Al_2O_3, CeO_2-ZrO_2, and TiO_2-ZrO_2) possessed higher surface areas, better reducibility, oxygen storage capacities, and enhanced sulfur dioxide resistance as compared with their single-component counterparts [23–26].

We envision that the support is used as the main adsorption site of SO_2, and noble metal(s) are loaded to improve catalytic activity and sulfur dioxide resistance of a catalyst. In the catalytic combustion of toluene in the presence of sulfur dioxide, SO_2 tends to be adsorbed on the active noble metal site, which deactivates the catalyst. Due to the interaction between the support and the active noble metal site, the sulfur dioxide resistance of a catalyst can be improved after suitable modification on the support and alloying of the noble metals. Therefore, we prepared the V_2O_5-TiO_2 composite support and its supported $PdPt_y$ NPs, in which V_2O_5 would act as the main adsorption site of SO_2, thus protecting the catalyst from being poisoned by SO_2. Hence, it is expected that the xPdPt$_y$/V_2O_5-TiO_2 (x and y are the PdPt$_y$ loading and Pt/Pd molar ratio, respectively) catalysts would exhibit excellent activity and good sulfur dioxide resistance. The purpose of this study was to design and prepare high-performance xPdPt$_y$/V_2O_5-TiO_2 catalysts with good moisture and sulfur dioxide resistance for the oxidation of toluene. The physical and chemical properties of these samples were measured using numerous techniques, and their catalytic performance was evaluated for toluene oxidation in the presence or absence of water, carbon dioxide, or sulfur dioxide. It was found that the well-dispersed $PdPt_{2.10}$ NPs, high adsorbed oxygen species concentration, good redox ability, large toluene adsorption capacity, and strong interaction between PdPt$_y$ and V_2O_5-TiO_2 were responsible for the

good catalytic performance of $0.46PdPt_{2.10}/V_2O_5$-TiO_2. Vanadium was the main site whereas PdO was the secondary site for SO_2 adsorption, which protected the active Pt site from being poisoned by SO_2, hence making the $0.46PdPt_{2.10}/V_2O_5$-TiO_2 catalyst exhibit good sulfur dioxide resistance.

2. Results and Discussion

2.1. Crystal Structure and Textural Property

The XRD technique was employed to measure the crystal phases and crystallinity of the samples. By referring to XRD patterns of the standard V_2O_5 (JCPDS PDF# 41-1426) and TiO_2 (JCPDS PDF# 21-1272) samples, we can realize that the diffraction peaks centered at 2θ = 15.4°, 20.4°, 21.7°, 26.2°, 31.0°, 34.3°, 41.2°, 48.2°, 51.2°, 54.1°, 55.2°, and 63.1° are assignable to the crystal phase of orthorhombic V_2O_5 (Figure 1a). Compared with the diffraction peaks of the V_2O_5 phase, the diffraction peaks of V_2O_5-TiO_2 decreased in intensity, which might be due to the formation of a solid solution structure in V_2O_5 and TiO_2. In addition, some diffraction peaks centered at 2θ = 25.3 ° and 37.8 ° were ascribable to the anatase TiO_2 phase (Figure 1b). The main peak indexes of the V_2O_5 and TiO_2 phases are shown in Figure 1f and g, respectively. After loading of Pt, Pd, or $PdPt_y$ NPs, there were orthorhombic V_2O_5 and anatase TiO_2 phases in the V_2O_5-TiO_2-supported noble metal samples, but the intensity of the diffraction peaks was significantly increased due to the rise in calcination temperature from 350 to 550 °C (Figure 1c–g). No significant noble metal phases were detected in XRD patterns of the supported samples, which means that the Pt, Pd, or $PdPt_y$ NPs are uniformly dispersed on the surface of V_2O_5-TiO_2.

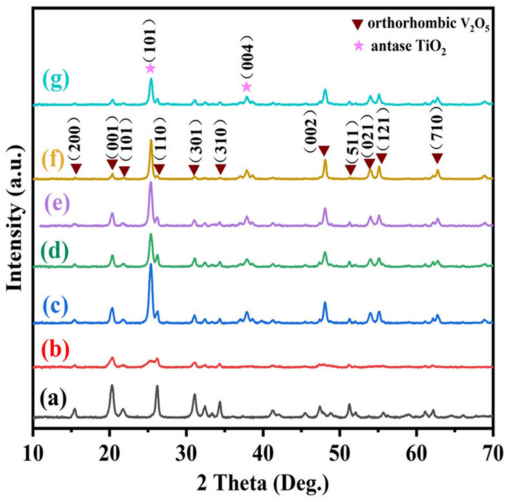

Figure 1. XRD patterns of (**a**) V_2O_5, (**b**) V_2O_5-TiO_2, (**c**) $0.47Pt/V_2O_5$-TiO_2, (**d**) $0.39Pd/V_2O_5$-TiO_2, (**e**) $0.46PdPt_{2.10}/V_2O_5$-TiO_2, (**f**) $0.41PdPt_{0.85}/V_2O_5$-TiO_2, and (**g**) $0.49PdPt_{0.44}/V_2O_5$-TiO_2.

Figure 2 shows TEM and HAADF-STEM images and elemental mappings of the samples as well as EDX line scan analysis of the $0.46PdPt_{2.10}/V_2O_5$-TiO_2 sample. The HADDF-STEM images and EDX elemental mappings of the as-obtained samples showed that the Pt, Pd, and $PdPt_y$ NPs were highly dispersed on the surface of V_2O_5-TiO_2. We also obtained line scanning data of the $0.46PdPt_{2.10}/V_2O_5$-TiO_2 sample, which showed that a bimetallic metal catalyst was successfully prepared. The SEM images of V_2O_5-TiO_2 are shown in Figure S1 (Supplementary Materials); the BET surface area, actual noble metal loadings, and Pt/Pd molar ratios of the samples are provided in Table 1; and the nitrogen adsorption–desorption isotherms and pore-size distributions of the samples are provided in Table 1 and Figure S2, respectively. It can be observed that surface areas (25.6–28.8 m^2/g) of the supported noble metal samples were slightly decreased, as compared with that (33.0 m^2/g) of V_2O_5-TiO_2.

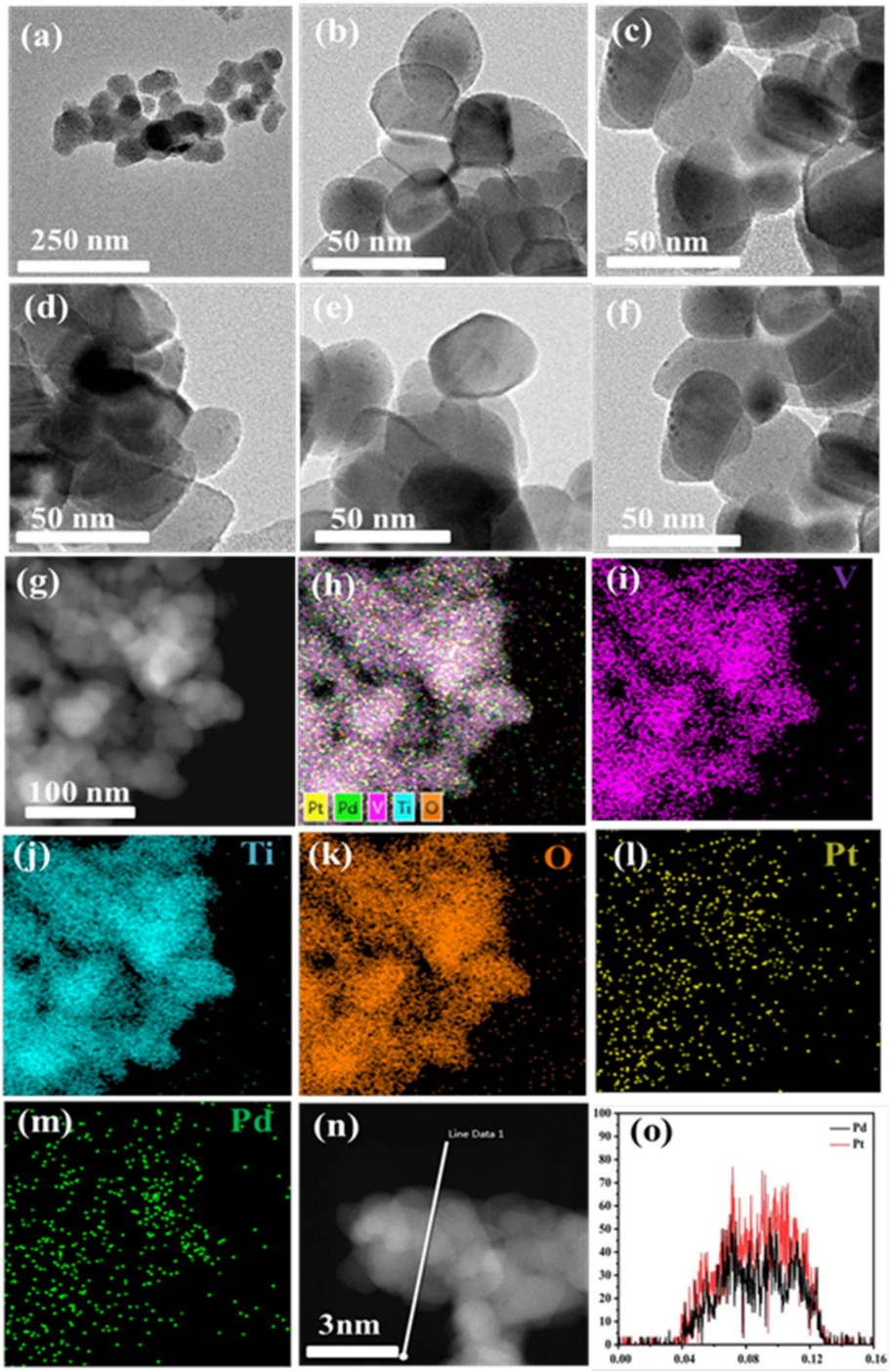

Figure 2. (**a**–**f**) TEM and (**g**,**n**) HAADF-STEM images, (**h**–**l**) elemental mappings, and (**o**) line-scan elemental analysis of (**a**) V_2O_5-TiO_2, (**b**) $0.46PdPt_{2.10}/V_2O_5$-TiO_2, (**c**) $0.41PdPt_{0.85}/V_2O_5$-TiO_2, (**d**) $0.49PdPt_{0.44}/V_2O_5$-TiO_2, (**e**) $0.47Pt/V_2O_5$-TiO_2, (**f**) $0.39Pd/V_2O_5$-TiO_2, and (**g**–**o**) $0.46PdPt_{2.10}/V_2O_5$-TiO_2.

Table 1. BET surface areas, pore volumes, pore diameters, actual noble metal contents, and actual Pt/Pd molar ratios of the as-prepared samples.

Sample	BET Surface Area [a] (m^2/g)	Pore Volume [a] (cm^3/g)	Pore Diameter [a] (nm)	Actual Noble Metal Content [b] (wt%)		Pt/Pd Molar Ratio (mol/mol)
				Pt	Pd	
V_2O_5-TiO_2	33.0	0.206	3.41	-	-	-
0.47Pt/V_2O_5-TiO_2	28.8	0.182	3.37	0.47	-	-
0.39Pd/V_2O_5-TiO_2	27.9	0.195	3.40	-	0.39	-
0.46PdPt$_{2.10}$/ V_2O_5-TiO_2	27.0	0.213	3.39	0.36	0.10	2.10
0.41PdPt$_{0.85}$/ V_2O_5-TiO_2	26.1	0.210	3.40	0.25	0.16	0.85
0.49PdPt$_{0.44}$/ V_2O_5-TiO_2	25.6	0.210	3.40	0.22	0.27	0.44

[a] Data were determined by the BET method; [b] data were determined by the ICP−AES technique.

2.2. Catalytic Performance

By using a gas chromatograph (GC-2014C, Shimadzu) with a FID, we detected the products of toluene oxidation over the 0.46PdPt$_{2.10}$/V_2O_5-TiO_2 sample at different temperatures and SV = 40,000 mL/(g h), and their gas chromatogram curves are shown in Figure S3. Obviously, there was only one signal that was assignable to toluene, and no other products were detected. In other words, no by-products (in addition to CO_2 and H_2O) were detected in the oxidation of toluene; i.e., CO_2 and H_2O selectivities were almost 100%. It should be noted that the intermediates with very low concentrations produced during the toluene oxidation could be detected using the in situ DRIFTS technique, which is more sensitive than the GC technique in detecting very low amounts of organics.

Catalytic toluene oxidation activities and Arrhenius plots of the samples are shown in Figure 3. Obviously, toluene conversion over each sample increased with the rise in temperature. The catalytic performance of V_2O_5-TiO_2 after loading of Pt, Pd, or PdPt$_y$ NPs was remarkably enhanced, as compared with that of the V_2O_5-TiO_2 support. Especially, the supported PdPt$_y$ bimetallic samples showed excellent catalytic activities. For the sake of convenient comparison, $T_{50\%}$ and $T_{90\%}$ (the reaction temperatures required when toluene conversion reaches 50% and 90%, respectively) are used to evaluate the catalytic activity. As can be seen from Figure 3A, 0.46PdPt$_{2.10}$/V_2O_5-TiO_2 performed the best ($T_{50\%}$ = 220 °C and $T_{90\%}$ = 245 °C at SV = 40,000 mL/(g h)).

In order to evaluate the catalyst activity more accurately, the $TOF_{Noble\ metal}$ and specific reaction rate of each catalyst at 230 °C were calculated, and the results are listed in Table 2. The $TOF_{Noble\ metal}$ increased in the order of 0.39Pd/V_2O_5-TiO_2 (12.0×10^{-3} s^{-1}) < 0.47Pt/V_2O_5-TiO_2 (17.4×10^{-3} s^{-1}) < 0.49PdPt$_{0.44}$/V_2O_5-TiO_2 (20.9×10^{-3} s^{-1}) < 0.41PdPt$_{0.85}$/V_2O_5-TiO_2 (56.8×10^{-3} s^{-1}) < 0.46PdPt$_{2.10}$/V_2O_5-TiO_2 (142.2×10^{-3} s^{-1}), same as the sequence in TOF_{Pd} or TOF_{Pt} of these samples. The specific reaction rate increased in the following sequence: 0.47Pt/V_2O_5-TiO_2 (34.8 μmol/(g_{Pt} s)) < 0.49PdPt$_{0.44}$/V_2O_5-TiO_2 (84.8 μmol/(g_{Pt} s)) < 0.41PdPt$_{0.85}$/V_2O_5-TiO_2 (85.6 μmol/(g_{Pt} s)) < 0.46PdPt$_{2.10}$/V_2O_5-TiO_2 (98.6 μmol/(g_{Pt} s)). It can be clearly seen that the sequence in specific reaction rate is basically consistent with that in catalytic activity of the samples. As shown in Table 2, the $TOF_{Noble\ metal}$ at 230 °C (17.4×10^{-3} s^{-1}) over 0.47Pt/V_2O_5-TiO_2 was higher than that (12.0×10^{-3} s^{-1}) over 0.39Pd/V_2O_5-TiO_2; i.e., the former outperformed the latter. Therefore, the sample with a higher Pt content showed a better catalytic activity than the one with a lower Pt content. That is to say, a decrease in Pt/Pd molar ratio in the sample led to a drop in catalytic activity.

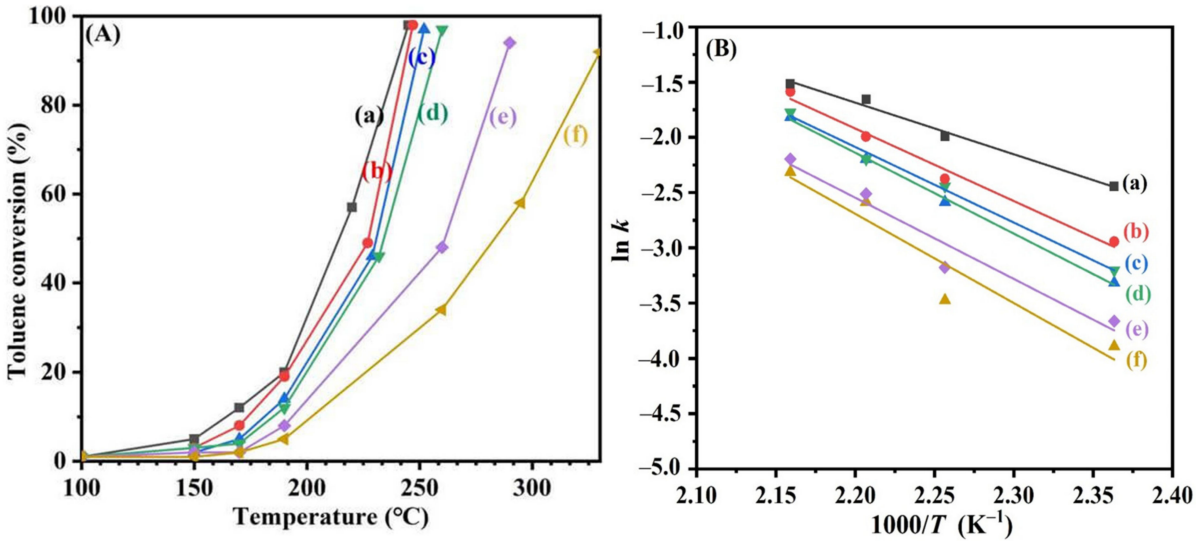

Figure 3. (**A**) Toluene conversion as a function of temperature and (**B**) ln k versus inverse temperature for (a) 0.46PdPt$_{2.10}$/V_2O_5-TiO_2, (b) 0.41PdPt$_{0.85}$/V_2O_5-TiO_2, (c) 0.49PdPt$_{0.44}$/V_2O_5-TiO_2, (d) 0.47Pt/V_2O_5-TiO_2, (e) 0.39Pd/V_2O_5-TiO_2, and (f) V_2O_5-TiO_2 for toluene oxidation at SV = 40,000 mL/(g h).

Table 2. Catalytic activities; specific reaction rates at 230 °C; TOF$_{Pd}$, TOF$_{Pt}$, and TOF$_{Noble\ metal}$ at 230 °C; metal dispersion; and apparent activation energies (E_a) of the samples for toluene oxidation at SV = 40,000 mL/(g h).

Sample	Catalytic Activity		Toluene Oxidation Activity at 230 °C				Metal Dispersion (%)	E_a (kJ/mol)
	$T_{50\%}$ (°C)	$T_{90\%}$ (°C)	Specific Reaction Rate (μmol/(g_{Pt} s))	TOF$_{Pd}$ ($\times 10^{-3}$ s^{-1})	TOF$_{Pt}$ ($\times 10^{-3}$ s^{-1})	TOF$_{Noble\ metal}$ ($\times 10^{-3}$ s^{-1})		
V_2O_5-TiO_2	295	330	-	-	-	-	-	68
0.39Pd/ V_2O_5-TiO_2	260	290	-	12.0	-	12.0	40	61
0.47Pt/ V_2O_5-TiO_2	228	252	34.8	-	17.4	17.4	39	59
0.49PdPt$_{0.44}$/ V_2O_5-TiO_2	230	260	84.8	21.1	47.2	20.9	35	54
0.41PdPt$_{0.85}$/ V_2O_5-TiO_2	225	247	85.6	56.9	66.1	56.9	25	51
0.46PdPt$_{2.10}$/ V_2O_5-TiO_2	220	245	98.6	134.9	68.7	142.2	28	45

The catalytic activities for toluene oxidation of 0.46PdPt$_{2.10}$/V_2O_5-TiO_2 prepared in the present work and various catalysts reported in the literature are compared in Table S1. According to the data in Table S1, the TOF$_{Noble\ metal}$ of 0.46PdPt$_{2.10}$/V_2O_5-TiO_2 at 230 °C was 142.2 $\times$ 10^{-3} s^{-1}, which was much higher than that (113.6 $\times$ 10^{-3} s^{-1}) of 0.5 wt% Pd/mesoporous ZrO_2 [27], that (125.2 $\times$ 10^{-3} s^{-1}) of 0.5 wt% Pt-WO_3/$Ce_{0.65}Zr_{0.35}O_2$ [28], and that (131.1 $\times$ 10^{-3} s^{-1}) of 1.71 wt% Pd/InO_x@CoO_x [29], but slightly lower than that (159.6 $\times$ 10^{-3} s^{-1}) of 1.0 wt% Pd/ZSM-5 [30] and that (146.8 $\times$ 10^{-3} s^{-1}) of 1.0 wt% Pd/Co_3AlO [31].

Xie et al. [32] studied the toluene oxidation kinetics over the AuPd/3DOM Mn_2O_3 catalyst and found that toluene oxidation followed a mechanism of first-order reaction toward toluene concentration (c) and a zero-order reaction toward oxygen concentration: $r = -kc = -A\exp(-E_a/(RT))c$, where r, A, k, and E_a are the reaction rate (mol/s), pre-exponential factor, rate constant (s^{-1}), and apparent activation energy (kJ/mol), respectively. Illustrated in Figure 3B are the Arrhenius plots for toluene oxidation over the samples at an SV of 40,000 mL/(g h), and the calculated E_a values are listed in Table 2. The E_a value increased in the order of 0.46PdPt$_{2.10}$/V_2O_5-TiO_2 (45 kJ/mol) < 0.41PdPt$_{0.85}$/V_2O_5-TiO_2 (51 kJ/mol) < 0.49PdPt$_{0.44}$/V_2O_5-TiO_2 (54 kJ/mol) < 0.47Pt/V_2O_5-TiO_2 (59 kJ/mol) < 0.39Pd/V_2O_5-TiO_2 (61 kJ/mol) < V_2O_5-TiO_2 (68 kJ/mol), with the 0.46PdPt$_{2.10}$$V_2O_5$-$TiO_2$ sample

exhibiting the lowest E_a value (45 kJ/mol), which was in good consistency with their activity changing trend.

2.3. Catalytic Stability and H_2O, CO_2, and SO_2 Resistance

There have been many reports on the effect of water vapor on catalytic activity [33]. For example, Zhang et al. [34] explored the effect of water on the methane oxidation activity of $0.44PtPd_{2.20}/ZrO_2$ and observed that the catalytic activity decreased owing to the introduction of water. In addition to the thermal stability, we also examined the effect of water vapor on the catalytic performance of $0.46PdPt_{2.10}/V_2O_5$-TiO_2 at SV = 40,000 mL/(g h), as shown in Figure 4A. Apparently, no significant changes in activity took place after 5.0 vol% water vapor was added to the reaction system. This demonstrates that the $0.46PdPt_{2.10}/V_2O_5$-TiO_2 sample possesses good water resistance. That is to say, toluene was more strongly adsorbed on the catalyst surface than water vapor, resulting in the catalytic activity not being affected significantly.

CO_2 is one of the products in toluene oxidation, and it can also influence the stability of a catalyst. For instance, Fu et al. [35] introduced 5.0 vol% CO_2 to the toluene combustion system over the $0.37Pt$-$0.16MnO_x$/meso-CeO_2 catalyst and observed that toluene conversion decreased slightly and such a partial deactivation was reversible. To explore the effect of CO_2 on catalytic activity, we introduced 5.0 vol% CO_2 to pass through the $0.46PdPt_{2.10}/V_2O_5$-TiO_2 sample at 245 °C and SV = 40,000 mL/(g h) and measured the resulting activities, as shown in Figure 4B. Obviously, the catalytic activity of toluene oxidation over $0.46PdPt_{2.10}/V_2O_5$-TiO_2 was not decreased significantly, which might be due to the fact that the alkalinity of the TiO_2 support is weaker [36], and the adsorption of CO_2 on TiO_2 and/or $PdPt_{2.10}$ NPs is also weaker. That is to say, the $0.46PdPt_{2.10}/V_2O_5$-TiO_2 sample exhibited good CO_2 resistance.

In some cases, there is the presence of a small amount of SO_2 in VOCs, which can poison the catalysts, thus resulting in an irreversible deactivation of the catalysts. After having monitored the changes in the activity of Pt/3DOM Mn_2O_3 for toluene combustion after introducing 40 ppm sulfur dioxide to the reaction system, Pei et al. [37] found that toluene conversion decreased significantly, which was due to the formation of the sulfate species that occupied the active sites. In other words, SO_2 addition induced an irreversible deactivation of the catalyst. One of the main aims of the present work is to prepare a support with good SO_2 resistance so that the sulfur resistance of the catalyst could be improved by competition for the adsorption of SO_2 with the active noble metal sites. As shown in Figure 4C–E, toluene oxidation experiments were conducted over V_2O_5-TiO_2, $0.47Pt/V_2O_5$-TiO_2, and $0.46PdPt_{2.10}/V_2O_5$-TiO_2 in the presence of 50 ppm SO_2 at SV = 40,000 mL/(g h). Obviously, toluene conversions first dropped slightly and then increased slightly over the V_2O_5-TiO_2 support after the introduction of 50 ppm SO_2. After 50 ppm SO_2 was introduced, toluene conversion over $0.47Pt/V_2O_5$-TiO_2 decreased rapidly, which was associated with the fact that SO_2 is adsorbed at the active Pt site, thus resulting in a decrease in active site amount for the adsorption of toluene and/or O_2. That is to say, SO_2 competed for the adsorption with reactants (toluene and oxygen). After about 4 h of reaction, the competitive adsorption of SO_2 and reactants at the active Pt site reached equilibrium, and toluene conversion decreased to 45%. When 50 ppm SO_2 was removed from the reaction system, toluene conversion was recovered to 90%. Over the $0.46PdPt_{2.10}/V_2O_5$-TiO_2 sample, however, a toluene conversion of 90% was still maintained after 50 ppm SO_2 was introduced, and the activity was restored to its initial conversion level when SO_2 was cut off. This result indicates that the support plays an important role in the sulfur resistance of a catalyst. The catalytic activity of $0.46PdPt_{2.10}/V_2O_5$-TiO_2 decreased slightly within 8 h of on-stream toluene oxidation at 245 °C after the addition of 50 ppm SO_2 and could return to its initial activity level after SO_2 provision was cut off. Therefore, we conclude that the use of the acidic V_2O_5-TiO_2 support as the main site of sulfur dioxide species adsorption can effectively improve the sulfur dioxide resistance of $0.46PdPt_{2.10}/V_2O_5$-TiO_2.

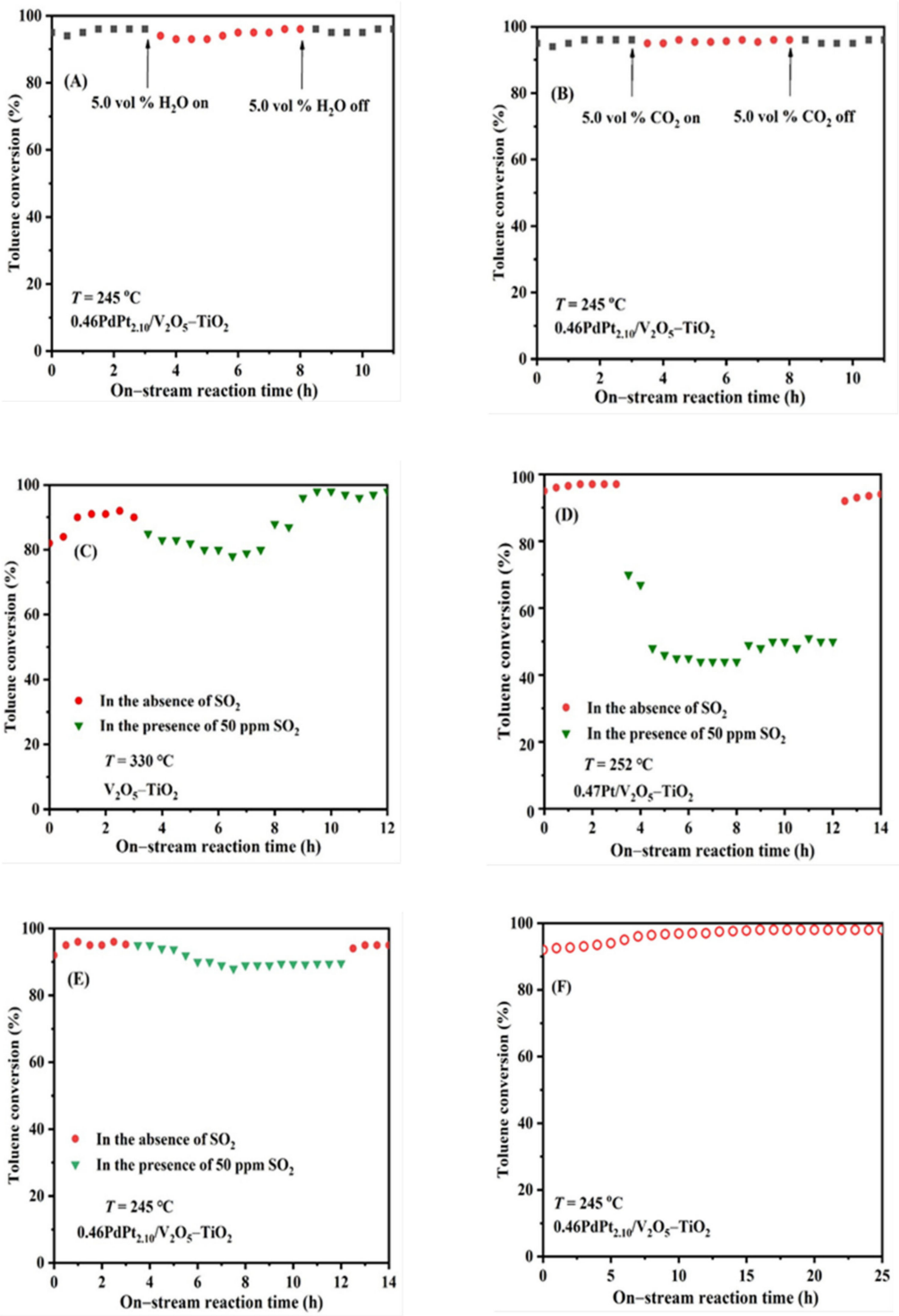

Figure 4. *Cont.*

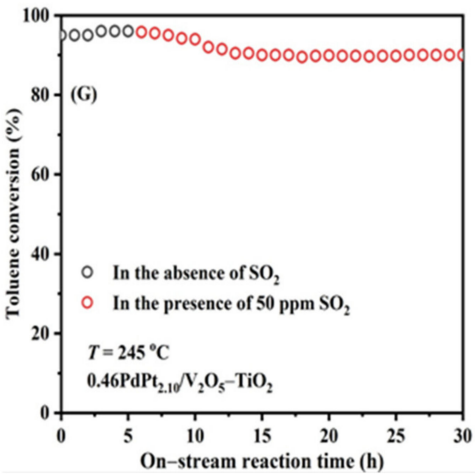

Figure 4. Effects of (**A**) 5.0 vol% H_2O and (**B**) 5.0 vol% CO_2 on catalytic activity of 0.46PdPt$_{2.10}$/V_2O_5-TiO_2; effect of 50 ppm SO_2 on catalytic activity of (**C**) V_2O_5-TiO_2, (**D**) 0.47Pt/V_2O_5-TiO_2, and (**E**) 0.46PdPt$_{2.10}$/V_2O_5-TiO_2; and catalytic activity versus on-stream reaction time in the (**F**) absence or (**G**) presence of 50 ppm SO_2 over 0.46PdPt$_{2.10}$/V_2O_5-TiO_2 for toluene oxidation at an SV of 40,000 mL/(g h).

We also investigated the thermal stability and sulfur dioxide resistance of the 0.46PdPt$_{2.10}$/V_2O_5-TiO_2 sample, and the results are shown in Figure 4F,G. Obviously, no significant drops in toluene conversion were observed within 25 h of on-stream reaction at 245 °C over 0.46PdPt$_{2.10}$/V_2O_5-TiO_2, indicating that the 0.46PdPt$_{2.10}$/V_2O_5-TiO_2 sample was stable under the dry and wet conditions. The TGA technique was used to analyze weight losses of the 0.46PdPt$_{2.10}$/V_2O_5-TiO_2 and 0.47Pt/V_2O_5-TiO_2 samples before and after 25 h of toluene oxidation in the presence of 50 ppm SO_2 at SV = 40,000 mL/(g h), and their TGA curves are shown in Figure S4. It can be seen that there was a gradual weight loss of ca. 0.7 wt% in the range of RT-600 °C for the fresh and used 0.46PdPt$_{2.10}$/V_2O_5-TiO_2 samples, which was due to the removal of the adsorbed reactants and CO_2 and H_2O; no weight loss due to the removal of the strongly adsorbed SO_2 on the sample surface was detected, demonstrating that the 0.46PdPt$_{2.10}$/V_2O_5-TiO_2 sample possessed a good resistance to SO_2. For the 0.47Pt/V_2O_5-TiO_2 sample after the sulfur dioxide treatment, however, a weight loss of ca. 0.7 wt% was observed in the range of 300–470 °C, which was owing to the decomposition of the strongly adsorbed SO_2 or the formed sulfite species, indicating that the 0.47Pt/V_2O_5-TiO_2 sample tended to be poisoned by SO_2.

To gain information on the physicochemical property change of the 0.46PdPt$_{2.10}$/V_2O_5-TiO_2 sample before and after 25 h of toluene oxidation in the presence of 50 ppm SO_2 at an SV of 40,000 mL/(g h), we measured the sample's XRD patterns, as shown in Figure S5. It can be seen that the crystal phase structure of the 0.46PdPt$_{2.10}$/V_2O_5-TiO_2 sample was not altered before and after 25 h of toluene oxidation in the presence of 50 ppm SO_2, which was in consistency with its stable catalytic performance. That is to say, the 0.46PdPt$_{2.10}$/V_2O_5-TiO_2 sample was durable under the adopted reaction conditions.

2.4. Surface Property

V 2p, Ti 2p, O 1s, S 2p, and Pt 4f XPS spectra of the fresh and SO_2-treated 0.47Pt/V_2O_5-TiO_2 and 0.46PdPt$_{2.10}$/V_2O_5-TiO_2 samples are shown in Figure 5, and their surface elemental compositions are listed in Table 3. The V 2p XPS spectrum of each sample was deconvoluted into three components at binding energy (BE) = 517.2, 515.9, and 515.4 eV (Figure 5A), which belonged to the surface V^{5+}, V^{4+}, and V^{3+} species [38–40], respectively. After SO_2 treatment, the $V^{5+}/V^{\gamma+}$ molar ratio decreased on 0.46PdPt$_{2.10}$/V_2O_5-TiO_2 and 0.47Pt/V_2O_5-TiO_2; i.e., there were greater amounts of V^{3+} and V^{4+} species on both SO_2-treated samples. As shown in Table 3, the S^{6+}/S^{4+} molar ratio (1.95) on the SO_2-treated 0.46PdPt$_{2.10}$/V_2O_5-TiO_2 sample was much higher than that (1.06) on the SO_2-treated

0.47Pt/V_2O_5-TiO_2 sample, indicating that there was a greater amount of sulfate species on the former than on the latter. The results suggest that electrons can be transferred from V to S (i.e., $V^{5+} + S^{4+} \Leftrightarrow V^{\gamma+} + S^{6+}$), indicating that after SO_2 treatment, vanadium could adsorb SO_2 to form vanadium sulfite and/or sulfate, thus protecting the active noble metal site to a certain extent. The Ti 2p XPS spectrum of each sample was divided into two components at BE = 458.4 and 464.1 eV (Figure 5B), which were assignable to the characteristic signal of the Ti^{4+} species [41]. Each of the O 1s XPS spectra could be decomposed into three components at BE = 529.7, 531.3, and 533.0 eV (Figure 5C), ascribable to the surface lattice oxygen (O_{latt}), adsorbed oxygen (O_{ads}), and adsorbed molecular water or carbonate species [42–44], respectively. As shown in Figure 5D, the two components at BE = 168.5 and 169.7 eV were attributable to the surface S^{6+} and S^{4+} species [45], respectively. After making the quantitative analysis, we can see that the 0.47Pt/V_2O_5-TiO_2 sample after SO_2 treatment shows a greater amount of sulfite and a lesser amount of sulfate, whereas the amounts of sulfite and sulfate on the 0.46PdPt$_{2.10}$/V_2O_5-TiO_2 sample after SO_2 treatment are just the opposite.

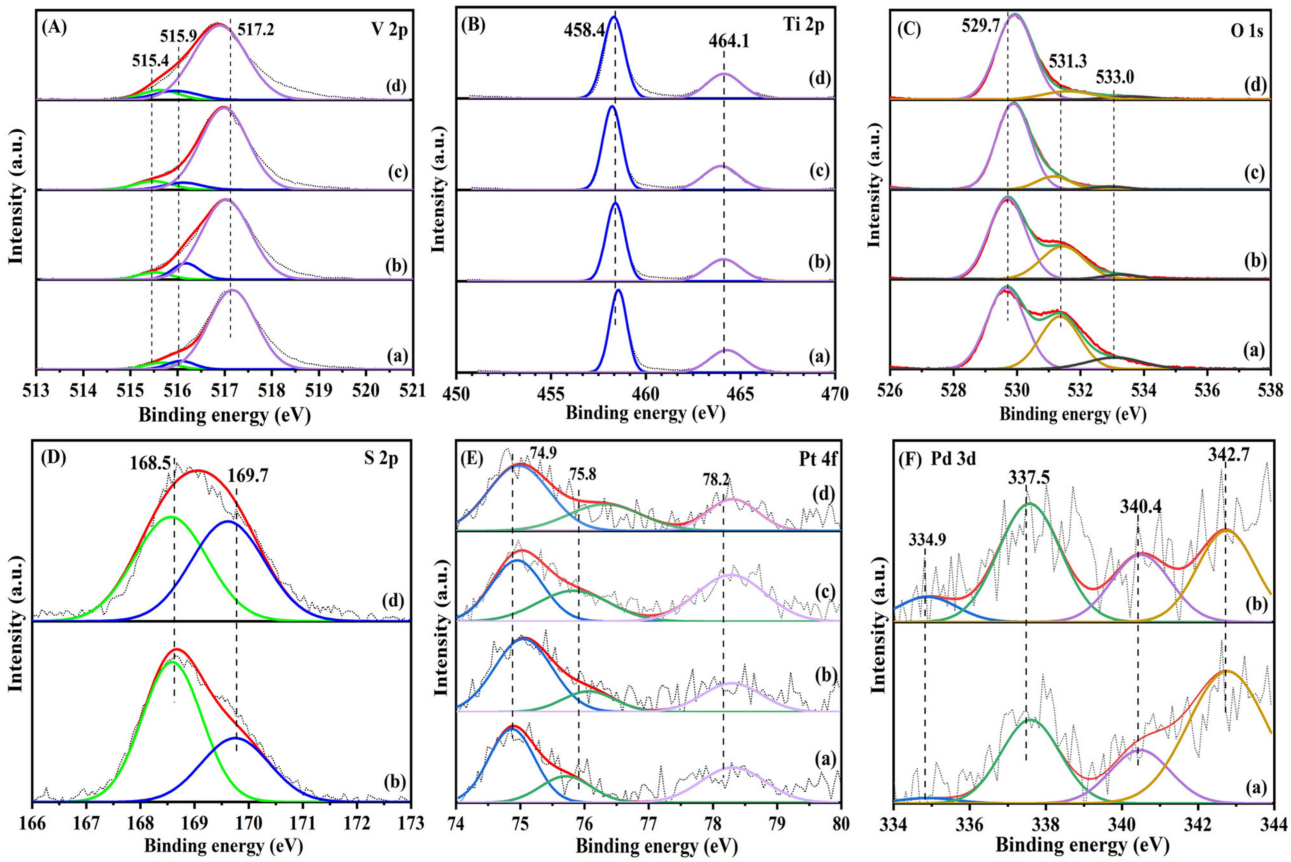

Figure 5. (**A**) V 2p, (**B**) Ti 2p, (**C**) O 1s, (**D**) S 2p, (**E**) Pt 4f, and (**F**) Pd 3d XPS spectra of (a) fresh 0.46PdPt$_{2.10}$/V_2O_5-TiO_2, (b) 0.46PdPt$_{2.10}$/V_2O_5-TiO_2 after SO_2 treatment, (c) fresh 0.47Pt/V_2O_5-TiO_2, and (d) 0.47Pt/V_2O_5-TiO_2 after SO_2 treatment.

Table 3. Surface element compositions and H_2 consumption of the fresh and SO_2-treated samples.

Sample	Surface Element Composition [a] (mol/mol)					H_2 Consumption at 150–400 °C [c] (mmol/g_{cat})
	Pd^0/Pd^{2+} Molar Ratio	Pt^{2+}/Pt^{4+} Molar Ratio	O_{ads}/O_{latt} Molar Ratio	$V^{5+}/V^{\gamma+}$ Molar Ratio [b]	S^{6+}/S^{4+} Molar Ratio	
0.39Pd/V_2O_5-TiO_2	0.80	-	0.10	4.21	-	1.20
0.47Pt/V_2O_5-TiO_2	-	0.30	0.22	6.66	0.00	1.08
0.49$PdPt_{0.44}$/V_2O_5-TiO_2	0.72	0.37	0.23	4.00	-	1.43
0.41$PdPt_{0.85}$/V_2O_5-TiO_2	0.65	0.35	0.27	5.00	-	1.70
0.46$PdPt_{2.10}$/V_2O_5-TiO_2	0.25	0.23	0.46	8.33	0.00	1.90
0.47Pt/V_2O_5-TiO_2 (used)	-	0.38	0.15	5.00	1.06	0.52
0.46$PdPt_{2.10}$/V_2O_5-TiO_2 (used)	0.43	0.24	0.44	5.26	1.95	1.80

[a] Data were obtained by quantitatively analyzing the peaks in XPS spectra of the samples; [b] $V^{\gamma+} = V^{3+} + V^{4+}$; [c] data were estimated by quantitatively analyzing the reduction peaks in the H_2-TPR profiles.

After curve fitting the Pt 4f spectrum of each sample, we can see three components at BE = 74.9, 75.8, and 78.2 eV (Figure 5E), among which the one at BE = 75.8 eV was ascribed to the surface oxidized Pt (Pt^{2+}) species, while the ones at BE = 74.9 and 78.2 eV were classified as the surface oxidized Pt (Pt^{4+}) species [46–49]. According to the quantitatively analyzed data listed in Table 3, we can see that the O_{ads}/O_{latt} molar ratio on the SO_2-treated 0.46$PdPt_{2.10}$/V_2O_5-TiO_2 sample decreased only slightly, and the Pt^{2+}/Pt^{4+} molar ratio increased slightly but the Pd^0/Pd^{2+} molar ratio increased remarkably from 0.25 to 0.43; however, the O_{ads}/O_{latt} molar ratio on the SO_2-treated 0.47Pt/V_2O_5-TiO_2 sample decreased considerably, and the Pt^{2+}/Pt^{4+} molar ratio increased markedly. The change in O_{ads}/O_{latt}, Pd^0/Pd^{2+}, or Pt^{2+}/Pt^{4+} molar ratio on the samples after SO_2 treatment might be associated with the adsorbed SO_2 species. Similarly, the Pd 3d spectrum of each Pd-containing sample was divided into four components: the two components at BE = 334.9 and 340.4 eV (Figure 5F) were assigned to the surface metallic Pd (Pd^0) species, whereas the other two components at BE = 337.5 and 342.7 eV were attributed to the surface oxidized Pd (Pd^{2+}) species [50,51]. The Pd^0/Pd^{2+} molar ratio increased because the sulfur dioxide could react with the surface lattice oxygen of PdO to form sulfur trioxide, which further consumed the lattice oxygen on the PdO surface [52]. In other words, the reaction of SO_2 with the O_{latt} on the PdO surface could promote the local reduction of PdO, resulting in an increase in the amount of the Pd^0 species on the sample surface.

The V 2p, Ti 2p, Pt 4f, Pd 3d, and O 1s XPS spectra of the 0.39Pd/V_2O_5-TiO_2, 0.49$PdPt_{0.44}$/V_2O_5-TiO_2, and 0.41$PdPt_{0.85}$/V_2O_5-TiO_2 samples are shown in Figure S6, and their surface elemental compositions are listed in Table 3. We notice that the O_{ads}/O_{latt} molar ratios on the $PdPt_y$-loaded samples were higher than that on the Pd- or Pt-loaded sample, with the 0.46$PdPt_{2.10}$/V_2O_5-TiO_2 sample exhibiting the highest O_{ads}/O_{latt} molar ratio (Table 3). That is to say, the 0.46$PdPt_{2.10}$/V_2O_5-TiO_2 sample possessed the strongest oxygen activation ability. In a sulfur-containing atmosphere, vanadium can compete with precious metals to adsorb SO_2 and protect the active Pt site from being poisoned by SO_2. It is hence understandable that the 0.46$PdPt_{2.10}$/V_2O_5-TiO_2 sample showed the highest activity in catalyzing the oxidation of toluene.

2.5. Reducibility and Oxygen Mobility

It is well known that the activity of a catalyst is associated with its low-temperature reducibility. Shown in Figure 6A are H_2-TPR profiles of the V_2O_5-TiO_2, 0.39Pd/V_2O_5-TiO_2, 0.47Pt/V_2O_5-TiO_2, 0.49PdPt$_{0.44}$/V_2O_5-TiO_2, 0.41PdPt$_{0.85}$/V_2O_5-TiO_2, and 0.46PdPt$_{2.10}$/V_2O_5-TiO_2 samples. Two reduction peaks were detected at 529 and 650 °C for the V_2O_5-TiO_2 support: the former was attributed to the reduction of the surface V^{5+} and Ti^{4+} to the V^{4+} and Ti^{3+} species, while the latter was ascribable to the reduction of the bulk V_2O_5 and TiO_2 species [53–55]. With the loading of Pt, Pd, or PdPt$_y$ NPs, the position of the reduction peak was shifted to a lower temperature, which was owing to the reduction of the oxidized noble metal in the supported sample. These results indicate that there is a strong interaction between Pt, Pd, or PdPt$_y$ NPs and V_2O_5-TiO_2. According to the quantitative analysis data (Table 3), we can realize that the loading of Pt, Pd, or PdPt$_y$ NPs on V_2O_5-TiO_2 causes the H_2 consumption of the sample to increase significantly. The reduction temperature of the 0.46PdPt$_{2.10}$/V_2O_5-TiO_2 sample was the lowest, indicating that this sample possessed the best low-temperature reducibility.

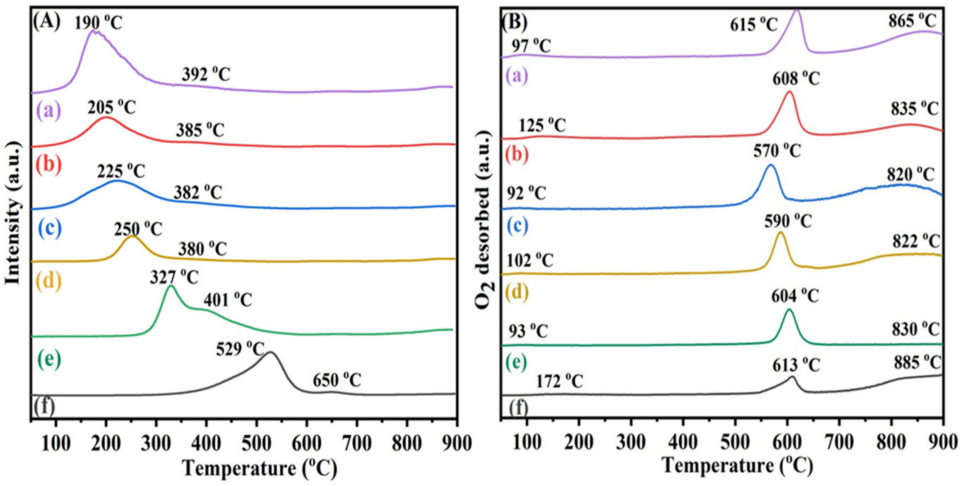

Figure 6. (**A**) H_2-TPR profiles and (**B**) O_2-TPD profiles of (a) 0.46PdPt$_{2.10}$/V_2O_5-TiO_2, (b) 0.41PdPt$_{0.85}$/V_2O_5-TiO_2, (c) 0.49PdPt$_{0.44}$/V_2O_5-TiO_2, (d) 0.47Pt/V_2O_5-TiO_2, (e) 0.39Pd/V_2O_5-TiO_2, and (f) V_2O_5-TiO_2.

Oxygen desorption behaviors of the samples were measured using the O_2-TPD technique, and their profiles are illustrated in Figure 6B and Figure S7. The peak in the low-temperature (<300 °C) region was considered as desorption of the chemically adsorbed O_{ads} (O_2^-, O_2^{2-}, or O^-) species and decomposition of the PtO_x, PdO_x, and $PtPdO_x$ species; the one in the range of 300–600 °C was classified as desorption of the surface O_{latt} species on V_2O_5-TiO_2; and the one above 600 °C was regarded as desorption of the bulk O_{latt} species in V_2O_5-TiO_2 [56]. Catalytic oxidation of toluene usually occurs below 600 °C. Hence, the main active oxygen species are the O_{ads} species and the O_{latt} species in noble metal oxides that were desorbed at lower temperatures. Of course, it cannot be ruled out that the surface O_{latt} species on V_2O_5-TiO_2 can participate in the oxidation of toluene at higher temperatures. Additionally, it should be noticed that the temperatures of oxygen desorption from the supported noble metal samples were shifted to lower temperatures as compared with those of the V_2O_5-TiO_2 support.

2.6. Toluene and Sulfur Dioxide Adsorption Behaviors

The adsorption of toluene on the catalyst is an important factor affecting its catalytic performance. The toluene-TPD experiments of the 0.47Pt/V_2O_5-TiO_2 and 0.46PdPt$_{2.10}$/V_2O_5-TiO_2 samples were carried out, and their desorption profiles are shown in Figure 7A. For each sample, there was one toluene desorption peak with weak chemisorption at 90 °C. The

$0.46PdPt_{2.10}/V_2O_5$-TiO_2 sample possessed the largest toluene desorption, suggesting that the sample can adsorb the largest amount of toluene, which is beneficial for the improvement in catalytic toluene oxidation activity. Figure 7B,C show MS spectra of carbon dioxide and water. It can be seen that when toluene is adsorbed on the sample surface, two different types of oxygen participate in the reaction. The peak at 90–300 °C was due to the reaction of the surface adsorbed oxygen species with toluene, while the one at 600–700 °C was owing to the reaction of the surface lattice oxygen species with toluene. The results were consistent with those of O_2-TPD characterization.

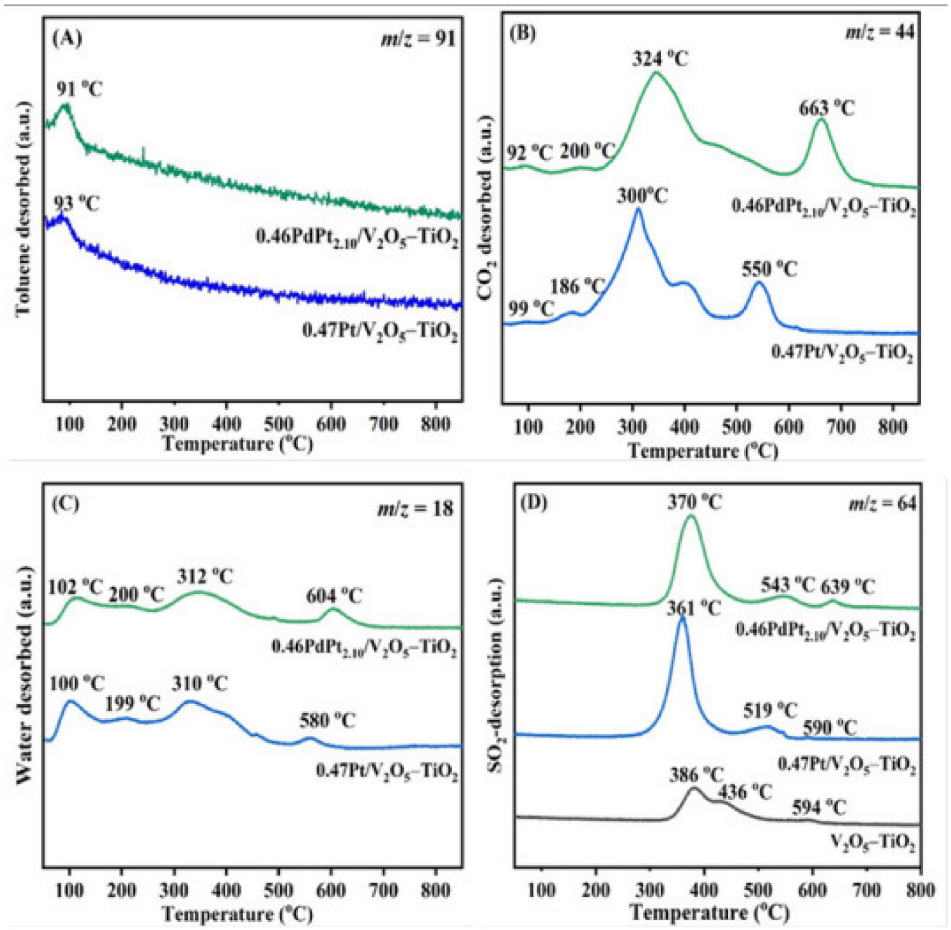

Figure 7. (**A**) Toluene, (**B**) CO_2, (**C**) water desorption in the toluene-TPD profiles, and (**D**) SO_2 desorption in (C_7H_8 + SO_2)-TPD profiles of $0.47Pt/V_2O_5$-TiO_2 and $0.46PdPt_{2.10}/V_2O_5$-TiO_2.

(C_7H_8 + SO_2)-TPD was used to investigate the thermal decomposition of the sulfate species on the sample surface after reaction, and their profiles are presented in Figure 7D. The V_2O_5-TiO_2, $0.47Pt/V_2O_5$-TiO_2, and $0.46PdPt_{2.10}/V_2O_5$-TiO_2 samples exhibited three desorption peaks. The desorption peak at 386 °C was due to the decomposition of the $V_2(SO_4)_3$ species, the one at 436 °C was assigned to the decomposition of the $VOSO_4$ species, and the one at 588 °C was ascribed to the decomposition of the $TiOSO_4$ species [57]. It is well known that the desorption peak below 400 °C is due to the decomposition of the weakly chemisorbed SO_2 and sulfite species, and the desorption peak above 400 °C is attributable to the decomposition of the strongly adsorbed sulfate species [58]. As revealed by the XPS characterization, the sulfate or sulfite species were formed on the surface of the sample after SO_2 treatment. The loading of precious metal NPs can make SO_2 be readily oxidized to SO_3. Additionally, vanadium competes with precious metals to adsorb sulfur oxide species, which can protect the active noble metal site from being poisoned by SO_2 or SO_3 to a certain extent. This means that the sulfate species produced at the

vanadium site are increased. From the (C_7H_8 + SO_2)-TPD results, we can see that the 0.47Pt/V_2O_5-TiO_2 sample possessed the largest amount of sulfur species desorption below 400 °C, which might be mainly due to the weak chemical adsorption of SO_2 on the Pt site, thus causing the sample to show a lower catalytic activity. Due to the enhanced Pt–Pd interaction, it was difficult for SO_2 to be adsorbed at the precious metal sites in the 0.46PdPt$_{2.10}$/V_2O_5-TiO_2 sample, thus protecting the active noble metal sites. In addition, we notice that the 0.46PdPt$_{2.10}$/V_2O_5-TiO_2 sample strongly adsorbs sulfur species to form vanadium sulfite or sulfate, and its desorption amount was larger as compared with that above 400 °C of the 0.47Pt/V_2O_5-TiO_2 sample, giving rise to a slight drop in catalytic activity. The desorption peak of the 0.46PdPt$_{2.10}$/V_2O_5-TiO_2 or 0.47Pt/V_2O_5-TiO_2 sample at about 370 °C significantly increased in intensity as compared with that of the V_2O_5-TiO_2 support. It is speculated that the catalyst may catalyze the oxidation of toluene in the sulfur-containing atmosphere, and vanadium is the main adsorption site of the sulfur species. Therefore, toluene conversion over the 0.47Pt/V_2O_5-TiO_2 sample was recovered to 90% after cutting off sulfur dioxide, while the activity of 0.46PdPt$_{2.10}$/V_2O_5-TiO_2 remained basically unchanged in the sulfur-containing atmosphere.

2.7. Adsorption Mechanisms of Toluene and Sulfur Dioxide

In order to determine whether the sulfate species are produced on the surface of the sample, we collected FT-IR spectra of the 0.47Pt/V_2O_5-TiO_2 (Figure 8A) and 0.46PdPt$_{2.10}$/V_2O_5-TiO_2 (Figure 8B) samples before and after toluene oxidation in the presence of 50 ppm SO_2 at SV = 40,000 mL/(g h) for 8 h. According to the assignments of absorption bands reported in the literature, we ascribe the band at 1115 cm^{-1} to the stretching vibration of the sulfite species [59]. There was a weak characteristic band assignable to the sulfite species at the noble metal sites in the SO_2-treated 0.46PdPt$_{2.10}$/V_2O_5-TiO_2 sample, which explains why the catalytic activity of this sample is not significantly altered. However, there was an obvious band at 1115 cm^{-1} attributable to the sulfite species at the noble metal site in the SO_2-treated 0.47Pt/V_2O_5-TiO_2 sample, and its catalytic activity was remarkably decreased as a result. In addition, the characteristic band at 1400 cm^{-1} increased in intensity, which was ascribable to the vibration mode of $VOSO_4$ after the sample was treated in the presence of SO_2. The vibration band intensity of the 0.46PdPt$_{2.10}$/V_2O_5-TiO_2 sample was stronger than that of the 0.47Pt/V_2O_5-TiO_2 sample, indicating that a greater amount of $VOSO_4$ was generated on the former sample, which protects the active noble metal site from being poisoned by SO_2 [60]. Therefore, the 0.46PdPt$_{2.10}$/V_2O_5-TiO_2 sample possessed a better sulfur dioxide–resistance ability.

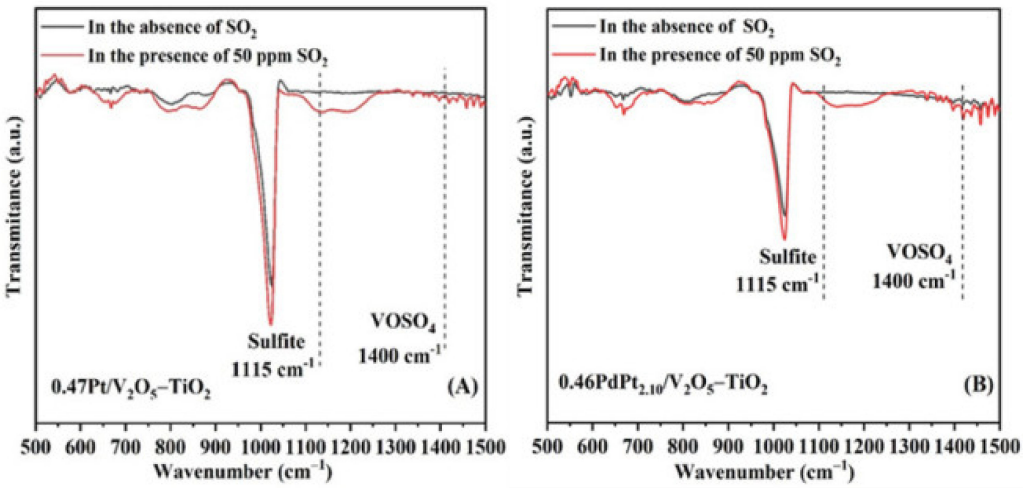

Figure 8. FT-IR spectra of the (**A**) 0.47Pt/V_2O_5-TiO_2 and (**B**) 0.46PdPt$_{2.10}$/V_2O_5-TiO_2 samples in the presence and absence of 50 ppm SO_2.

In situ DRIFTS experiments were conducted to elucidate the formation and changes of the surface species on the 0.47Pt/V_2O_5-TiO_2 and 0.46PdPt$_{2.10}$/V_2O_5-TiO_2 samples during the toluene oxidation process at different temperatures or reaction times. The adsorption process was undertaken in a (1000 ppm toluene + 20 vol% O_2 + N_2 (balance)) mixture flow at different temperatures, and the as-obtained in situ DRIFTS spectra of the 0.47Pt/V_2O_5-TiO_2 and 0.46PdPt$_{2.10}$/V_2O_5-TiO_2 samples are shown in Figure 9A,C, respectively. The characteristic absorption band at 3040 cm^{-1} was attributed to the C–H bond stretching vibration of the aromatic ring in toluene, and the one at 2935 cm^{-1} was assigned to the asymmetric stretching vibration of the C–H bond of methyl in toluene [61]. The characteristic absorption band at 1498 cm^{-1} was caused by the planar skeleton vibration of the benzene ring [62]. It can be seen from Figure 9A,C that the characteristic band gradually disappeared with the rise in temperature. This result indicates that toluene is completely oxidized. According to the assignment of the characteristic absorption bands [63–65], we detected signals of the surface adsorbed C=O (at 1642 cm^{-1}), anhydride (at 1850 cm^{-1}), COO– (at 1545 cm^{-1}), carboxylic acid (at 1380 cm^{-1}), H_2O (at 3653 and 3836 cm^{-1}), chemisorbed oxygen (at 1050 cm^{-1}), and other minor species during the toluene oxidation process. These results demonstrate that *p*-methylbenzoquinone is formed during the toluene oxidation process, and anhydride, benzoic acid, and benzaldehyde are further generated with the extension of the reaction. Finally, CO_2 and H_2O were produced with the rise in temperature.

In order to investigate the difference of adsorbed species on the sample surface during the toluene oxidation process in the presence of 50 ppm SO_2, we first activated the 0.47Pt/V_2O_5-TiO_2 or 0.46PdPt$_{2.10}$/V_2O_5-TiO_2 sample in an oxygen flow at 250 °C for 1 h, and we then recorded in situ DRIFTS spectra of the adsorbed species at different times and 270 °C. As shown in Figure 9B,D, the absorption band at 1160 cm^{-1} was attributed to the vibration of SO_4^{2-}, whereas the one at 970 cm^{-1} was assigned to the vibration of SO_3^{2-} [66]. As shown in Figure 9C, the intensity of the absorption band at 970 cm^{-1} of 0.47Pt/V_2O_5-TiO_2 was significantly higher than that of 0.46PdPt$_{2.10}$/V_2O_5-TiO_2, indicating that SO_2 is adsorbed on the active Pt site in the sample to form the sulfite species. With the progress of the reaction, we can also see that the characteristic bands (at 2935 and 3040 cm^{-1}) owing to toluene are significantly enhanced, indicating that the introduction of SO_2 competes the adsorption with toluene at the active site, and the oxidation of toluene was decreased. However, there was no obvious change in the characteristic band of toluene (Figure 9D), indicating that the toluene oxidation activity of the 0.46PdPt$_{2.10}$/V_2O_5-TiO_2 sample was not affected by the introduction of SO_2. As revealed in the XPS and (C_7H_8 + SO_2)-TPD characterization, SO_2 was mainly adsorbed at the vanadium site to form sulfate on the 0.46PdPt$_{2.10}$/V_2O_5-TiO_2 sample after SO_2 treatment. In addition, the doping of Pt with Pd could also protect the active Pt site from being poisoned by SO_2, making the 0.46PdPt$_{2.10}$/V_2O_5-TiO_2 sample show better sulfur dioxide resistance.

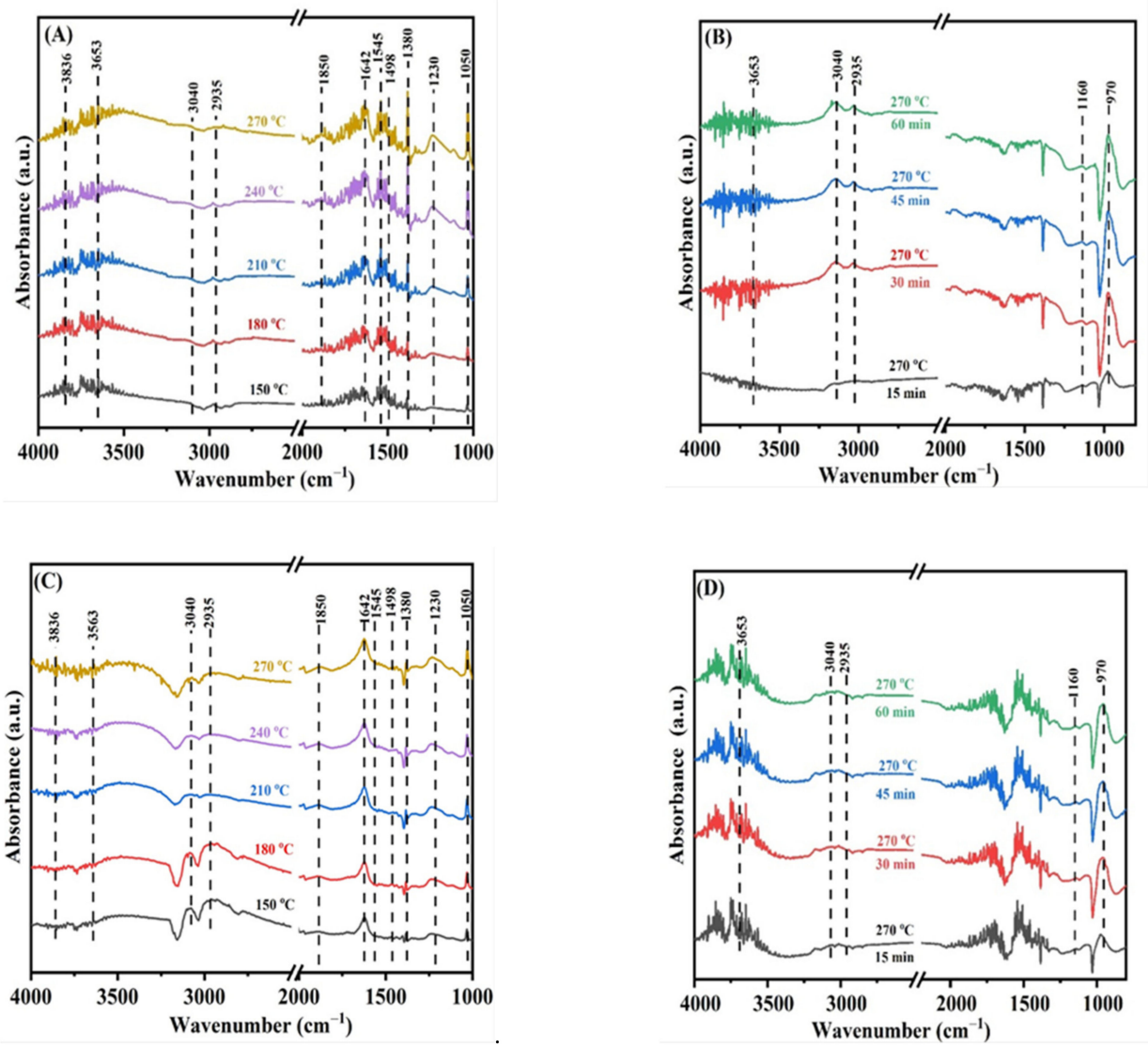

Figure 9. In situ DRIFTS spectra of (**A**,**B**) 0.47Pt/V_2O_5-TiO_2 and (**C**,**D**) 0.46Pd$Pt_{2.10}$/V_2O_5-TiO_2 for (**A**,**C**) C_7H_8 at different temperatures and (**B**,**D**) (C_7H_8 + SO_2) oxidation at different times (after activation treatment in an O_2 flow at 250 °C).

3. Materials and Methods

3.1. Catalyst Preparation

3.1.1. Preparation of the V_2O_5-TiO_2 Support

The V_2O_5-TiO_2 composite support was prepared using the hydrothermal method. In a typical preparation, 2.5 g of V_2O_5 powder was added to 5.0 g of oxalic acid dissolved in 40 mL of deionized (DI) water, and the as-obtained suspension was then stirred at 85 °C for 4 h. After being cooled to room temperature (RT), the resulting blue aqueous solution was added dropwise to 30 mL of an isopropanol solution under stirring for 2 h. The above mixture was poured into an autoclave for thermal treatment at 180 °C for 20 h. After the thermally treated mixture was washed with 48 mL of DI water and ethanol (DI water/ethanol volumetric ratio = 5:1), centrifuged, and dried in an oven at 80 °C for 8 h, the as-obtained dried solid was calcined in a muffle furnace at a ramp of 3 °C/min from RT to 350 °C and kept at this temperature for 2 h, and thus the V_2O_5 was obtained. Then, 0.6 g of the as-obtained V_2O_5 was dissolved in 50 mL of ethanol under stirring for 30 min, followed by the addition of 0.1 g of hydroxypropyl cellulose (HPC) under stirring for 30 min. Five milliliters of tetrabutyl titanate (TBOT) was dissolved in 30 mL of ethanol under stirring for 30 min. After that, the TBOT-containing ethanol solution was added to the above

V_2O_5-HPC-containing ethanol solution under stirring for 1 h. The resulting solution was washed with 35 mL of DI water, centrifuged, and dried in an oven at 80 °C for 8 h. The obtained solid was thermally treated in a muffle furnace at a ramp of 3 °C/min from RT to 350 °C and kept at 350 °C for 2 h; hence, obtaining the V_2O_5-TiO_2 composite support.

3.1.2. Preparation of xPt/V_2O_5-TiO_2, xPd/V_2O_5-TiO_2, and xPdPt_y/V_2O_5-TiO_2

1.42 mL of $PdCl_2$ or 2.58 mL of H_2PtCl_6 aqueous solution (Pd or Pt/PVA mass ratio = 1.5:1.0 mg/mg) was added to 2.0 mL of polyvinyl alcohol (PVA) aqueous solution (2.0 g/L) in an ice–water bath and protected from being illuminated by light. After being magnetically stirred for 30 min, 1.60 or 2.93 mL of $NaBH_4$ aqueous solution (2.0 g/L; Pd or Pt/$NaBH_4$ molar ratio = 1.0:5.0 mol/mol) was rapidly added to the above precursor aqueous solution under stirring, and a Pd or Pt sol was obtained after stirring for 30 min. At this time, the solution turned brown black. A desired amount of V_2O_5-TiO_2 was added to the above-obtained Pd or Pt sol. After that, the mixture was stirred for 8 h, and the precipitate was filtered with a funnel, washed with 2.0 L of DI water and 1.0 L of ethanol to remove the Cl^- and Na^+ ions as well as the PVA adsorbed on the catalyst surface, and dried at 80 °C for 12 h. The dried solid was calcined in a muffle furnace at a ramp of 3 °C/min from RT to 550 °C and maintained at 550 °C for 6 h, and thus obtaining the supported Pd or Pt nanocatalyst. According to the results of the characterization by inductively coupled plasma atomic emission spectroscopy (ICP-AES), we can know that the actual loadings (x) of Pt and Pd in the supported samples were 0.43 and 0.49 wt%, and the obtained samples were denoted as 0.47 Pt/V_2O_5-TiO_2 and 0.39 Pd/V_2O_5-TiO_2, respectively.

The preparation procedures for xPdPt_y/V_2O_5-TiO_2 (x and y are the PdPt_y loading and Pt/Pd molar ratio, respectively) were similar to those of the above-mentioned 0.43Pt/V_2O_5-TiO_2 or 0.49Pd/V_2O_5-TiO_2 sample. Typically, 1.20, 0.90, or 0.62 mL of H_2PtCl_6 and 0.52, 0.90, or 1.43 mL of $PdCl_2$ aqueous solution (Pt and Pd/PVA mass ratio = 1.0:1.5 mg/mg; theoretical Pt/Pd molar ratio = 7:3, 1:1, and 3:7) were added to 2 mL of the PVA aqueous solution (2.0 g/L) in an ice–water bath, which was protected from being illuminated by light. After being magnetically stirred for 30 min, 1.4, 2.1, or 2.3 mL of $NaBH_4$ aqueous solution (2.0 g/L; PdPt_y/$NaBH_4$ molar ratio = 1.0:5.0 mol/mol) was rapidly added to the above precursor aqueous solution under stirring. The other preparation steps were the same as those for the preparation of 0.47Pt/V_2O_5-TiO_2 or 0.39Pd/V_2O_5-TiO_2. The ICP-AES results reveal that the actual loadings (x) of PdPt_y in xPdPt_y/V_2O_5-TiO_2 are 0.46, 0.41, and 0.49 wt%, and the actual Pt/Pd molar ratios (y) are 2.10, 0.85, and 0.44, respectively. Therefore, the as-obtained catalysts were denoted as 0.46Pd$Pt_{2.10}$/V_2O_5-TiO_2, 0.41Pd$Pt_{0.85}$/V_2O_5-TiO_2, and 0.49Pd$Pt_{0.44}$/V_2O_5-TiO_2, respectively. It should be noted that during the process of loading noble metal NPs on V_2O_5-TiO_2, the washing treatment could lead to the loss of some precious metals, thus resulting in the difference between the nominal and actual metal loadings.

3.2. Catalyst Characterization

Physical and chemical properties of the samples were determined by means of techniques such as ICP-AES (Thermo Electron IRIS Intrepid ER/S spectrometer, Waltham, MA, USA); metal dispersion measurements; X-ray diffraction (XRD, Bruker/AXS D8 Advance diffractometer, with Cu Kα radiation and nickel filter (λ = 0.15406 nm), Berlin, Germany); transmission electron microscopy (TEM, JEOL JEM-2010, Tokyo, Japan); high-angle annular dark-field scanning transmission electron microscopy (HAADF-STEM, FEI G280-200/Chemi-STEM, Potsdam, Germany); nitrogen adsorption–desorption (BET, Micromeritics ASAP 2020 analyzer, Norcross, GA, USA); thermogravimetric analysis (TGA, Setaram Labsys evo, Caluire, France); X-ray photoelectron spectroscopy (XPS, Thermo Fisher Scientific ESCALAB 250 Xi spectrometer, Waltham, MA, USA); toluene, (sulfur dioxide + toluene), and oxygen temperature-programmed desorption (toluene-, (SO_2 + C_7H_8)-, and O_2-TPD (Autochem II 2920, Micromeritics, Norcross, GA, USA), respectively); hydrogen temperature-programmed reduction (H_2-TPR, AutoChem II 2920, Micromeritics,

Norcross, GA, USA); Fourier transform infrared spectroscopy (ATR-FTIR, TENSOR II, Bruker, Berlin, Germany) and in situ diffuse reflectance infrared Fourier transform spectroscopy (in situ DRIFTS, Nicolet 6700 FT-IR spectrometer with a liquid-nitrogen-cooled MCT detector, Bruker, Berlin, Germany). The detailed characterization procedures are stated in the Supplementary Materials.

3.3. Catalytic Evaluation

Catalytic activities of the samples were measured in a continuous flow fixed-bed quartz tubular microreactor (i.d. = 6.0 mm) at atmospheric pressure. A Shimadzu gas chromatograph (GC-2014C) was used for online analysis of the concentrations of the gases in the outlet of the microreactor. We loaded 25 mg of the sample well mixed with 125 mg of quartz sand (particle size: 40–60 mesh) in the microreactor. An O_2 flow of 20 mL/min was introduced into the microreactor, and the sample was pretreated at 250 °C for 1 h. The reactant gas mixture was composed of (1000 ppm toluene + 20 vol% O_2 + N_2 (balance)), and the space velocity (SV) was 40,000 mL/(g h). In the water, carbon dioxide, or sulfur dioxide resistance test, 5.0 vol% water vapor, 5.0 vol% CO_2, or 50 ppm SO_2 (N_2 as the balance gas) was introduced to the reaction system over the typical sample at 245 °C. We adopted the temperatures at toluene conversions of 50% and 90% ($T_{50\%}$ and $T_{90\%}$, respectively) to evaluate the catalytic activity of each sample. The specific reaction rate and turnover frequencies (TOF_{Pd}, TOF_{Pt}, or $TOF_{Noble\ metal}$) at a given temperature were also calculated. The detailed procedures for activity evaluation are described in the Supplementary Materials.

4. Conclusions

The V_2O_5-TiO_2 composite support was first prepared via a hydrothermal route, and the 0.39Pd/V_2O_5-TiO_2, 0.47Pt/V_2O_5-TiO_2, 0.46PdPt$_{2.10}$/V_2O_5-TiO_2, 0.41PdPt$_{0.85}$/V_2O_5-TiO_2, and 0.49PdPt$_{0.44}$/V_2O_5-TiO_2 samples were then obtained using the PVA-protecting $NaBH_4$ reduction method. Among all of the as-obtained samples, 0.46PdPt$_{2.10}$/V_2O_5-TiO_2 showed the best catalytic activity: $T_{50\%}$ = 220 °C and $T_{90\%}$ = 245 °C at SV = 40,000 mL/(g h), E_a = 45 kJ/mol, TOF_{Pt} at 230 °C = 68.7 × 10^{-3} s^{-1}, and specific reaction rate at 230 °C = 98.6 μmol/(g_{Pt} s). The good catalytic performance of 0.46PdPt$_{2.10}$/V_2O_5-TiO_2 was associated with its well-dispersed PdPt$_{2.10}$ NPs, high adsorbed oxygen species concentration, good redox ability, large toluene adsorption capacity, and strong interaction between PdPt$_y$ and V_2O_5-TiO_2. Furthermore, the 0.46PdPt$_{2.10}$/V_2O_5-TiO_2 sample showed excellent thermal stability, water resistance, and CO_2 resistance. When 50 ppm SO_2 was added to the feedstock, toluene conversions over V_2O_5-TiO_2, 0.47Pt/V_2O_5-TiO_2, and 0.46PdPt$_{2.10}$/V_2O_5-TiO_2 decreased from 95% to 76%, 45%, and 90%, respectively; when 50 ppm SO_2 was cut off, however, catalytic activities over the three samples were basically recovered. It is concluded that in the preparation of the sulfur dioxide-resistant V_2O_5-TiO_2 composite support, vanadium played a role as the main site for SO_2 adsorption, thus protecting the active Pt site in 0.46PdPt$_{2.10}$/V_2O_5-TiO_2 from being poisoned by SO_2.

Supplementary Materials: Supplementary data associated with this article can be found at https://https://www.mdpi.com/article/10.3390/catal12111302/s1, Catalyst characterization procedures. Catalytic activity evaluation procedures. Figure S1: SEM images of the V_2O_5-TiO_2 support. Figure S2: (A) Nitrogen adsorption–desorption isotherms and (B) pore-size distributions of (a) V_2O_5-TiO_2, (b) 0.39Pd/V_2O_5-TiO_2, (c) 0.47Pt/V_2O_5-TiO_2, (d) 0.49PdPt$_{0.44}$/V_2O_5-TiO_2, (e) 0.41PtPt$_{0.85}$/V_2O_5-TiO_2, and (f) 0.46PdPt$_{2.10}$/V_2O_5-TiO_2. Figure S3: Gas chromatogram curves of toluene oxidation at (A) RT, (B) 170 °C, (C) 220 °C, and (D) 245 °C over the 0.46PdPt$_{2.10}$/V_2O_5-TiO_2 sample at SV = 40,000 mL/(g h). Figure S4: TGA curves of the fresh and used 0.46PdPt$_{2.10}$/V_2O_5-TiO_2 and 0.47Pt/V_2O_5-TiO_2 samples before and after 25 h of reaction in the presence of 50 ppm SO_2 at SV = 40,000 mL/(g h). Figure S5: XRD patterns of (a) the fresh 0.46PdPt$_{2.10}$/V_2O_5-TiO_2 sample, (b) the used 0.46PdPt$_{2.10}$/V_2O_5-TiO_2 sample after 25 h of toluene oxidation in the absence of 50 ppm SO_2, and (c) the used 0.46PdPt$_{2.10}$/V_2O_5-TiO_2 sample after 25 h of toluene oxidation in the presence of 50 ppm SO_2 at an SV of 40,000 mL/(g h). Figure S6: (A) V 2p, (B) Ti 2p, (C) O 1s,

(D) Pt 4f, and (E) Pd 3d XPS spectra of (a) $0.41PdPt_{0.85}/V_2O_5$-TiO_2, (b) $0.49PdPt_{0.44}/V_2O_5$-TiO_2, and (c) $0.39Pd/V_2O_5$-TiO_2. Figure S7: Partially enlarged O_2-TPD profiles of (a) $0.46PdPt_{2.10}/V_2O_5$-TiO_2, (b) $0.41PdPt_{0.85}/V_2O_5$-TiO_2, (c) $0.49PdPt_{0.44}/V_2O_5$-TiO_2, (d) $0.47Pt/V_2O_5$-TiO_2, (e) $0.39Pd/V_2O_5$-TiO_2, and (f) V_2O_5-TiO_2. Table S1: Comparison of catalytic activities for toluene combustion of the $0.46PdPt_{2.10}/V_2O_5$-TiO_2 catalyst obtained in the present work and the various catalysts reported in the literature. References [27–31] are cited in the supplementary materials.

Author Contributions: Conceptualization, H.D.; Methodology, H.D.; Software, J.S.; Investigation, J.S.; Resources, H.D.; Data Curation, J.S., Y.L., J.D. and L.J.; Writing—Original Draft Preparation, J.S.; Writing—Review and Editing, H.D.; Visualization, M.B., Q.S., L.L., L.W. and X.H.; Supervision, H.D.; Project Administration, H.D.; Funding Acquisition, H.D. All authors have read and agreed to the published version of the manuscript.

Funding: This work was supported by the National Natural Science Committee of China—Liaoning Provincial People's Government Joint Fund (No. U1908204), National Natural Science Foundation of China (Nos. 21876006, 21976009, and 21961160743), Foundation on the Creative Research Team Construction Promotion Project of Beijing Municipal Institutions (No. IDHT20190503), Natural Science Foundation of Beijing Municipal Commission of Education (No. KM201710005004), and Development Program for the Youth Outstanding—Notch Talent of Beijing Municipal Commission of Education (No. CIT&TCD201904019).

Data Availability Statement: All the relevant data used in this study have been provided in the form of figures and tables in the published article, and all data provided in the present manuscript are available to whom they may concern.

Conflicts of Interest: The authors declare no conflict of interest.

References

1. He, C.; Cheng, J.; Zhang, X.; Douthwaite, M.; Pattisson, S.; Hao, Z.P. Recent advances in the catalytic oxidation of volatile organic compounds: A review based on pollutant sorts and sources. *Chem. Rev.* **2019**, *119*, 4471–4568. [CrossRef]
2. Zhang, C.; Guo, Y.; Guo, Y.; Lu, G.; Boreave, A.; Retailleau, L.; Baylet, A.; Giroir-Fendler, A. $LaMnO_3$ perovskite oxides prepared by different methods for catalytic oxidation of toluene. *Appl. Catal. B* **2014**, *148–149*, 490–498. [CrossRef]
3. Ministry of Environment. *Contents of New Emission Regulation of Volatile Organic Compounds*; Ministry of Environment, Government of Japan: Tokyo, Japan, 2005.
4. Kamal, M.S.; Razzak, S.A.; Hossain, M.M. Catalytic oxidation of volatile organic compounds (VOCs)—A review. *Atmos. Environ.* **2016**, *140*, 117–134. [CrossRef]
5. Zhang, Z.X.; Jiang, Z.; Shangguan, W.F. Low-temperature catalysis for VOCs removal in technology and application: A state-of-the-art review. *Catal. Today* **2016**, *264*, 270–278. [CrossRef]
6. Liotta, L.F. Catalytic oxidation of volatile organic compounds on supported noble metals. *Appl. Catal. B* **2010**, *100*, 403–412. [CrossRef]
7. Peng, R.; Sun, X.; Li, S.J.; Chen, L.M.; Fu, M.L.; Wu, J.L.; Ye, D.Q. Shape effect of Pt/CeO_2 catalysts on the catalytic oxidation of toluene. *Chem. Eng.* **2016**, *306*, 1234–1246. [CrossRef]
8. Rui, Z.B.; Tang, M.N.; Ji, W.K.; Ding, J.J.; Ji, H.B. Insight into the enhanced performance of TiO_2 nanotube supported Pt catalyst for toluene oxidation. *Catal. Today* **2017**, *297*, 159–166. [CrossRef]
9. Wang, H.; Yang, W.; Tian, P.H.; Zhou, J.; Tang, R.; Wu, S.J. A highly active and anti-coking Pd-Pt/SiO_2 catalyst for catalytic combustion of toluene at low temperature. *Appl. Catal. A* **2017**, *529*, 60–67. [CrossRef]
10. Ordoez, S.; Hurtado, P.; Sastre, H. Methane catalytic combustion over Pd/Al_2O_3 in presence of sulphur dioxide: Development of a deactivation model. *Appl. Catal. A* **2004**, *259*, 41–48. [CrossRef]
11. Zhu, H.F.; Ma, L.; Li, X.N. Progress of the preparation of sulfur-tolerant palladium catalyst for catalytic oxidation of methane. *Appl. Chem. Ind.* **2018**, *47*, 2231–2241.
12. Chenakin, S.P.; Melaet, G.; Szukiewicz, R.; Kruse, N. XPS study of the surface chemical state of a $Pd/(SiO_2+TiO_2)$ catalyst after methane oxidation and SO_2 treatment. *J. Catal.* **2014**, *312*, 1–11. [CrossRef]
13. Xie, S.X.; Yu, Y.B.; Wang, J.; He, H. Effect of SO_2 on the performance of Ag-Pd/Al_2O_3 for the selective catalytic reduction of NO_x with C_2H_5OH. *Environ. Sci.* **2006**, *18*, 973–978. [CrossRef]
14. Venezia, A.M.; Carlo, G.D.; Liotta, L.F.; Pantaleo, G.; Kantcheva, M. Effect of Ti(IV) loading on CH_4 oxidation activity and SO_2 tolerance of Pd catalysts supported on silica SBA-15 and HMS. *Appl. Catal. B* **2011**, *106*, 529–539. [CrossRef]
15. Ryou, Y.; Lee, J.; Lee, H.; Choung, J.W.; Yoo, S.; Kim, D.H. Roles of ZrO_2 in SO_2-poisoned $Pd/(Ce\text{-}Zr)O_2$ catalysts for CO oxidation. *Catal. Today* **2015**, *258*, 518–524. [CrossRef]

16. Xia, M.R.; Yue, R.L.; Chen, P.X.; Wang, M.Q.; Jiao, T.F.; Zhang, L.; Zhao, Y.F.; Gao, F.F.; Wei, Z.D.; Li, L. Density functional theory investigation of the adsorption behaviors of SO_2 and NO_2 on a Pt(111) surface. *Colloids Surf. A Physicochem. Eng. Asp.* **2019**, *568*, 266–270. [CrossRef]
17. Ball, D.J.; Stack, R.G.; Crucq, A. Catalysis and Automotive Pollution Control II. *Stud. Surf. Sci. Catal.* **1991**, *71*, 337–351.
18. Hoyos, L.J.; Praliaud, H.; Primet, M. Catalytic combustion of methane over palladium supported on alumina and silica in presence of hydrogen sulfide. *Appl. Catal. A* **1993**, *98*, 125–138. [CrossRef]
19. Lapina, O.B.; Bal'zhinimaev, B.S.; Boghosian, S.; Eriksen, K.M.; Fehrmann, R. Progress on the mechanistic understanding of SO_2 oxidation catalysts. *Catal. Today* **1999**, *51*, 469–479. [CrossRef]
20. Mamiyev, Z.; Dillert, R.; Zheng, N.; Bahnemann, D.W. Rh/TiO_2-photocatalyzed acceptorless dehydrogenation of N-heterocycles upon visible-light illumination. *ACS Catal.* **2020**, *10*, 5542–5553.
21. Balayeva, N.O.; Zheng, N.; Dillert, R.; Bahnemann, D.W. Visible-light-mediated photocatalytic aerobic dehydrogenation of N-heterocycles by surface-grafted TiO_2 and 4-amino-TEMPO. *ACS Catal.* **2019**, *12*, 10694–10704. [CrossRef]
22. Balayeva, N.O.; Fleisch, M.; Bahnemann, D.W. Surface-grafted WO_3/TiO_2 photocatalysts: Enhanced visible-light activity towards indoor air purification. *Catal. Today* **2018**, *313*, 63–71. [CrossRef]
23. Wang, W.Y.; Yang, Y.Q.; Luo, H.; Wang, T.F.; Liu, W.Y. Ultrasound-assisted preparation of titania–alumina support with high surface area and large pore diameter by modified precipitation method. *Alloys Compd.* **2011**, *509*, 3430–3434. [CrossRef]
24. Gu, Z.H.; Luo, L.T.; Chen, S.F. Effect of calcinations temperature of TiO_2-Al_2O_3 mixed oxides on hydrodesulphurization performance of Au-Pd catalysts. *Chem. Technol.* **2009**, *16*, 175–180.
25. Gomez-Garcí, M.A.; Pitchon, V.; Kiennemann, A. Multifunctional catalysts for de-NO_x processes: The case of $H_3PW_{12}O_{40}\cdot 6H_2O$-metal supported on mixed oxides. *Appl. Catal. B* **2007**, *70*, 151–159. [CrossRef]
26. Gomez-Garcí, M.A.; Thomas, S.; Pitchon, V.; Kiennemann, A. Selective reduction of NO_x by liquid hydrocarbons with supported HPW-metal catalysts. *Catal. Today* **2007**, *119*, 52–58. [CrossRef]
27. Tidahy, H.L.; Hosseni, M.; Siffert, S.; Cousin, R.; Lamonier, J.F.; Aboukaïs, A.; Su, B.L.; Giraudon, J.M.; Leclercq, G. Nanostructured macro-mesoporous zirconia impregnated by noble metal for catalytic total oxidation of toluene. *Catal. Today* **2008**, *137*, 335–339. [CrossRef]
28. Hou, Z.X.; Zhou, X.Y.; Lin, T.; Chen, Y.Q.; Lai, X.X.; Feng, J.; Sun, M.M. The promotion effect of tungsten on monolith Pt/$Ce_{0.65}Zr_{0.35}O_2$ catalysts for the catalytic oxidation of toluene. *New J. Chem.* **2019**, *43*, 5719–5726. [CrossRef]
29. Du, X.B.; Dong, F.; Tang, Z.C.; Zhang, J.Y. Precise design and synthesis of Pd/InO_x@CoO_x core–shell nanofibers for the highly efficient catalytic combustion of toluene. *Nanoscale* **2020**, *12*, 12133–12145. [CrossRef]
30. He, C.; Shen, Q.; Liu, M.X. Toluene destruction over nanometric palladium supported ZSM-5 catalysts: Influences of support acidity and operation condition. *J. Porous Mater.* **2014**, *21*, 551–563. [CrossRef]
31. Li, P.; He, C.; Cheng, J.; Ma, C.Y.; Dou, B.J.; Hao, Z.P. Catalytic oxidation of toluene over Pd/Co_3AlO catalysts derived from hydrotalcite-like compounds: Effects of preparation methods. *Appl. Catal. B* **2011**, *101*, 570–579. [CrossRef]
32. Xie, S.H.; Liu, Y.X.; Deng, J.G.; Zhao, X.T.; Yang, J.; Zhang, K.F.; Han, Z.; Arandiyan, H.; Dai, H.X. Effect of transition metal doping on the catalytic performance of Au–Pd/3DOM Mn_2O_3 for the oxidation of methane and *o*-xylene. *Appl. Catal. B* **2017**, *206*, 221–232. [CrossRef]
33. Yin, F.X.; Ji, S.F.; Wu, P.Y.; Zhao, F.Z.; Li, C.Y. Preparation, characterization, and methane total oxidation of $AAl_{12}O_{19}$ and $AMAl_{11}O_{19}$ hexaaluminate catalysts prepared with urea combustion method. *J. Mol. Catal. A* **2008**, *294*, 27–36. [CrossRef]
34. Zhang, X.F.; Liu, Y.X.; Deng, J.G.; Jing, L.; Wu, L.K.; Dai, H.X. Catalytic performance and SO_2 resistance of zirconia-supported platinum-palladium bimetallic nanoparticles for methane combustion. *Catal. Today* **2022**, *402*, 0920–5861. [CrossRef]
35. Fu, X.H.; Liu, Y.X.; Deng, J.G.; Jing, L.; Zhang, X.; Zhang, K.F.; Han, Z.; Jiang, X.Y.; Dai, H.X. Intermetallic compound $PtMn_y$-derived Pt–MnO_x supported on mesoporous CeO_2: Highly efficient catalysts for the combustion of toluene. *Appl. Catal. A* **2020**, *595*, 117509.
36. Tumuluri, U.; Howe, J.D.; Mounfield, W.P., III; Li, M.J.; Chi, M.F.; Hood, Z.D.; Walton, K.S.; Sholl, D.S.; Dai, S.; Wu, Z.L. Effect of Surface Structure of TiO_2 Nanoparticles on CO_2 Adsorption and SO_2 Resistance. *Sustain. Chem. Eng.* **2017**, *10*, 9295–9306. [CrossRef]
37. Pei, W.B.; Liu, Y.X.; Deng, J.G.; Zhang, K.F.; Hou, Z.Q.; Zhao, X.T.; Dai, H.X. Partially embedding Pt nanoparticles in the skeleton of 3DOM Mn_2O_3: An effective strategy for enhancing catalytic stability in toluene combustion. *Appl. Catal. B* **2019**, *256*, 117814. [CrossRef]
38. Yang, W.; Liu, F.; Xie, L.; Lian, Z.; He, H. Effect of V_2O_5 additive on the SO_2 resistance of a Fe_2O_3/AC catalyst for NH_3-SCR of NOx at low temperatures. *Ind. Eng. Chem. Res.* **2016**, *55*, 2677–2685. [CrossRef]
39. Zhou, X.; Huang, X.; Xie, A.; Luo, S.; Yao, C.; Li, X.; Zuo, S. V_2O_5-decorated Mn-Fe/attapulgite catalyst with high SO_2 tolerance for SCR of NO_x with NH_3 at low temperature. *Chem. Eng. J.* **2017**, *326*, 1074–1085. [CrossRef]
40. Zhang, S.L.; Zhong, Q. Promotional effect of WO_3 on O^{2-} over V_2O_5/TiO_2 catalyst for selective catalytic reduction of NO with NH_3. *J. Mol. Catal. A* **2013**, *373*, 108–113. [CrossRef]
41. Rasmi, K.R.; Vanithakumari, S.C.; George, R.P.; Mallika, C.; Mudali, U.K. Nanoparticles of Pt loaded on a vertically aligned TiO_2 nanotube bed: Synthesis and evaluation of electrocatalytic activity. *RSC Adv.* **2015**, *5*, 108050–108057.
42. Deng, W.; Dai, Q.G.; Lao, Y.J.; Shi, B.B.; Wang, X.Y. Low temperature catalytic combustion of 1,2-dichlorobenzene over CeO_2–TiO_2 mixed oxide catalysts. *Appl. Catal. B* **2016**, *181*, 848–861. [CrossRef]

43. Rousseau, S.; Loridant, S.; Delichere, P.; Boreave, A.; Deloume, J.P.; Vernoux, P. $La_{(1-x)}Sr_xCo_{1-y}Fe_yO_3$ perovskites prepared by sol–gel method: Characterization and relationships with catalytic properties for total oxidation of toluene. *Appl. Catal. B* **2009**, *88*, 438–447. [CrossRef]
44. Xie, S.H.; Deng, J.G.; Zang, S.M.; Yang, H.G.; Guo, G.S.; Arandiyan, H.; Dai, H.X. Preparation and high catalytic performance of Au/3DOM Mn_2O_3 for the oxidation of carbon monoxide and toluene. *J. Catal.* **2015**, *322*, 38–48. [CrossRef]
45. Mitome, J.; Karakas, G.; Bryan, A.K.; Ozkan, U.S. Effect of H_2O and SO_2 on the activity of Pd/TiO_2 catalysts in catalytic reduction of NO with methane in the presence of oxygen. *Catal. Today* **1998**, *42*, 3–11. [CrossRef]
46. Peng, R.S.; Li, S.J.; Sun, X.B.; Ren, Q.M.; Chen, L.M.; Fu, M.L.; Wu, J.L.; Ye, D.Q. Size effect of Pt nanoparticles on the catalytic oxidation of toluene over Pt/CeO_2 catalysts. *Appl. Catal. B* **2018**, *220*, 462–470. [CrossRef]
47. Chen, C.Y.; Wang, X.; Zhang, J.; Pan, S.X.; Bian, C.Q.; Wang, L.; Chen, F.; Meng, X.J.; Zheng, X.M.; Gao, X.H.; et al. Superior Performance in Catalytic Combustion of Toluene over KZSM-5 Zeolite Supported Platinum Catalyst. *Catal. Today* **2014**, *144*, 1851–1859. [CrossRef]
48. Bera, P.; Priolkar, K.R.; Gayen, A.; Sarode, P.R.; Hegde, M.S.; Emura, S.; Kumashiro, R.; Jayaram, V.; Subbanna, G.N. Ionic Dispersion of Pt over CeO_2 by the Combustion Method: Structural Investigation by XRD, TEM, XPS, and EXAFS. *Chem. Mater.* **2003**, *15*, 2049–2060. [CrossRef]
49. Chen, L.X.; Sterbinsky, G.E.; Tait, S.L. Synthesis of Platinum Single-Site Centers through Metal-Ligand Self-Assembly on Powdered Metal Oxide Supports. *J. Catal.* **2018**, *365*, 303–312. [CrossRef]
50. Li, Y.B.; Zhang, C.B.; Ma, J.Z.; Chen, M.; Deng, H.; He, H. High temperature reduction dramatically promotes Pd/TiO_2 catalyst for ambient formaldehyde oxidation. *Appl. Catal. B* **2017**, *217*, 560–569. [CrossRef]
51. Jabłonsk, M.; Krol, A.; Kukulska-Zajac, E.; Tarach, K.; Girman, V.; Chmielarz, L.; Gora-Marek, K. Zeolites Y modified with palladium as effective catalysts for low temperature methanol incineration. *Appl. Catal. B* **2015**, *166*, 353–365. [CrossRef]
52. Monai, M.; Montini, T.; Melchionna, M.; Duchoň, T.; Kúš, P.; Chen, C.; Tsud, N.; Nasi, L.; Prince, K.C.; Veltruská, K.; et al. The effect of sulfur dioxide on the activity of hierarchical Pd-based catalysts in methane combustion. *Appl. Catal. B* **2017**, *202*, 72–83. [CrossRef]
53. Gao, X.T.; Bare, S.R.; Fierro, J.; Wachs, I.E. Structural characteristics and reactivity/ reducibility properties of dispersed and bilayered V_2O_5/TiO_2/SiO_2 catalysts. *J. Phys. Chem. B* **1999**, *103*, 618–629. [CrossRef]
54. Ayandiran, A.A.; Bakare, I.A.; Binous, H.; Al-Ghamdi, S.; Razzak, S.A.; Hossain, M.M. Oxidative dehydrogenation of propane to propylene over VO_x/CaO–γ-Al_2O_3 using lattice oxygen. *Catal. Sci. Technol.* **2016**, *6*, 5154–5167. [CrossRef]
55. Wang, Y.; Zhao, J.; Wang, X.; Li, Z.; Liu, P. The complete oxidation of ethanol at low temperature over a novel Pd-Ce/γ-Al_2O_3-TiO_2 catalyst. *Bull. Korean Chem. Soc.* **2013**, *34*, 2461–2465. [CrossRef]
56. Han, L.; Gao, M.; Hasegawa, J.; Li, S.; Shen, Y.; Li, H.; Shi, L.; Zhang, D. SO_2-Tolerant Selective Catalytic Reduction of NO_x over Meso-TiO_2@Fe_2O_3@Al_2O_3 Metal-Based Monolith Catalysts. *Environ. Sci. Technol.* **2019**, *53*, 6462–6473. [CrossRef]
57. Lowell, P.S.; Schwitzgebel, K.; Parsons, T.B.; Sladek, K.J. Selection of Metal Oxides for Removing SO_2 From Flue Gas Industrial. *Eng. Chem. Process Des. Dev.* **1971**, *10*, 384–390. [CrossRef]
58. Zhang, K.Y.; Dai, L.Y.; Liu, Y.X.; Deng, J.G.; Jing, L.; Zhang, K.F.; Hou, Z.Q.; Zhang, X.; Wang, J.; Feng, Y.; et al. Insights into the active sites of chlorine-resistant Pt-based bimetallic catalysts for benzene oxidation. *Appl. Catal. B* **2020**, *279*, 119372. [CrossRef]
59. Mitchell, M.B.; Sheinker, V.N.; White, M.G. Adsorption and Reaction of Sulfur Dioxide on Alumina and Sodium-Impregnated Alumina. *J. Phys. Chem.* **1996**, *100*, 7550–7557. [CrossRef]
60. Khodayari, R.; Odenbrand, C.U.I. Regeneration of commercial SCR catalysts by washing and sulphation: Effect of sulphate groups on the activity. *Appl. Catal. B* **2001**, *33*, 277–291. [CrossRef]
61. Zhao, S.; Hu, F.Y.; Li, J.H. Hierarchical core-shell Al_2O_3@Pd-CoAlO microspheres for low-temperature toluene combustion. *ACS Catal.* **2016**, *6*, 3433–3441. [CrossRef]
62. Huang, S.Y.; Zhang, C.B.; He, H. Complete oxidation of *o*-xylene over Pd/Al_2O_3 catalyst at low temperature. *Catal. Today* **2008**, *139*, 15–23. [CrossRef]
63. Liu, X.L.; Zeng, J.L.; Shi, W.B.; Wang, J.; Zhu, T.Y.; Chen, Y.F. Catalytic oxidation of benzene over ruthenium cobalt bimetallic catalysts and study of its mechanism. *Catal. Sci. Technol.* **2017**, *7*, 213–221. [CrossRef]
64. Zhang, X.; Dai, L.Y.; Liu, Y.X.; Deng, J.G.; Li, J.; Wang, Z.W.; Pei, W.B.; Yu, X.H.; Wang, J.; Dai, H.X. Effect of support nature on catalytic activity of the bimetallic RuCo nanoparticles for the oxidative removal of 1,2-dichloroethane. *Appl. Catal. B* **2021**, *285*, 119804. [CrossRef]
65. Rainone, F.; Bulushev, D.A.; Kiwi-Minsker, L.; Renken, A. DRIFTS and transient-response study of vanadia/titania catalysts during toluene partial oxidation. *Phys. Chem. Chem. Phys.* **2003**, *5*, 4445–4449. [CrossRef]
66. Wilburn, M.S.; Epling, W.S. Formation and decomposition of sulfite and sulfate species on Pt/Pd catalysts: An SO_2 oxidation and sulfur exposure study. *ACS Catal.* **2019**, *9*, 640–648. [CrossRef]